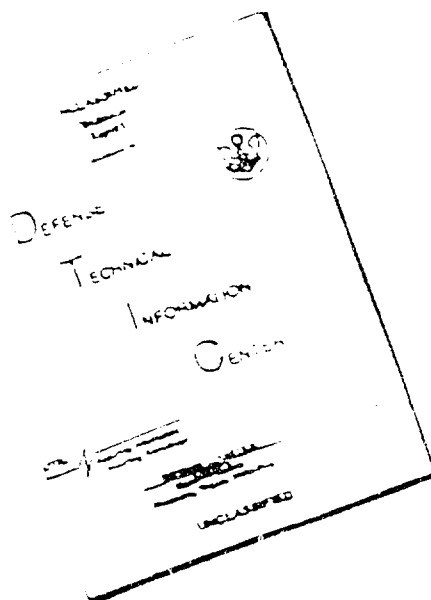# UNCLASSIFIED

AD 283 991

Reproduced
by the

ARMED SERVICES TECHNICAL INFORMATION AGENCY
ARLINGTON HALL STATION
ARLINGTON 12, VIRGINIA

UNCLASSIFIED

DISCLAIMER NOTICE

THIS DOCUMENT IS BEST QUALITY AVAILABLE. THE COPY FURNISHED TO DTIC CONTAINED A SIGNIFICANT NUMBER OF PAGES WHICH DO NOT REPRODUCE LEGIBLY.

283 991

AFOSR 3025

SHOCK TUNNEL STUDIES OF HIGH ENTHALPY IONIZED AIRFLOWS

By: A.Q. Eschenroeder, J.W. Daiber,
T.C. Golian, and A. Hertzberg
Contract No. AF 49(638)-952
CAL Report No. AF-1500-A-1
July 1962

CORNELL AERONAUTICAL LABORATORY, INC.

OF CORNELL UNIVERSITY, BUFFALO 21, N.Y.
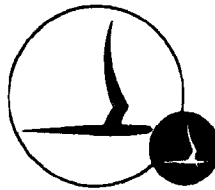
CORNELL AERONAUTICAL LABORATORY, INC.
BUFFALO 21, NEW YORK

REPORT NO. AF-1500-A-1

SHOCK TUNNEL STUDIES OF HIGH-ENTHALPY IONIZED AIRFLOWS

JULY 1962

CONTRACT NO. AF 49(638)-952

BY: _A. Q. Eschenroeder_

A. Q. Eschenroeder

J. W. Daiber

J. W. Daiber

T. C. Golian

T. C. Golian

A. Hertzberg

A. Hertzberg

PREPARED FOR:
MECHANICS DIVISION
AIR FORCE OFFICE OF SCIENTIFIC RESEARCH
OF THE
OFFICE OF AEROSPACE RESEARCH
WASHINGTON, D. C.

ASTIA

SEP 19 1962
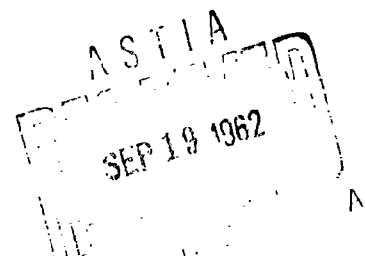
FOREWORD

This work, conducted at Cornell Aeronautical Laboratory, was sponsored by the Office of Scientific Research, Mechanics Division, under Contract AF 49(638)-952; by the Office of Naval Research, Mathematical Sciences Division under Contract Nonr 2653(00); and by Cornell Aeronautical Laboratory Internal Research.

The material in this report was presented at the AGARD Meeting on High Temperature Aspects of Hypersonic Fluid Dynamics in Brussels, Belgium, 3 - 6 April 1962.

AF-1500-A-1

ABSTRACT

Recent developments in shock tunnel techniques have permitted experimentation in hypersonic airflows having very high enthalpies. In the present paper, the Cornell Aeronautical Laboratory six-foot shock tunnel will be described, the effects of nonequilibrium flow in such a device will be assessed, and high-enthalpy experiments involving nozzle ionization will be discussed.

The six-foot shock tunnel at the Cornell Aeronautical Laboratory utilizes heated high-pressure hydrogen for a driver gas to obtain hypersonic airflows at high stagnation temperatures and pressures. Reflected shock operation is used with the tailored-interface technique to maximize the duration of steady flow. A significant portion of re-entry flight conditions can be duplicated for various hypersonic vehicles; however, partial simulation may be used to cover a far wider range of velocity and altitude. For measuring ionization levels and collision frequencies, microwave diagnostics have been recently employed.

Owing to the high degrees of initial dissociation and the large expansion of the test gas, it has been necessary to study the influences of nonequilibrium chemistry and ionization on the conditions in the test section. To this end, a general numerical code has been developed for an IBM 704 computer in order to solve quasi-one-dimensional flows with coupled rate processes. Such theoretical studies are essential for planning and interpreting experiments in high-temperature tunnel flows. Solutions have been obtained for airflows with atoms, molecules, electrons, and ions reacting simultaneously. Investigations of various ion kinetic machanisms have shown that processes such

as charge transfer, impact ionization, and mutual neutralization may play significant roles under certain conditions of hypersonic flow in shock tunnels and about blunt bodies in flight.

Preliminary experiments carried out in the shock tunnel have dealt with nonequilibrium ionization. Phase shift of microwaves passed through the airflow in the tunnel nozzle has yielded information on deionization kinetics and on the duration of useful test flow. Critical frequencies far below the microwave band are indicated for the gas over the entire range of conditions in the test section. These experiments have indicated that flows of high enthalpy can be generated by shock tunnels for the detailed study of the ionized shock layer on a hypersonic vehicle.

TABLE OF CONTENTS

AF-1500-A-1

LIST OF TABLES

LIST OF FIGURES

AF-1500-A-1

I. INTRODUCTION

Recent interest in phenomena associated with objects entering the earth's atmosphere at high velocities has stimulated research in the field of nonequilibrium flows. In many cases a more detailed knowledge of physico-chemical processes is needed than for purely aerodynamic effects because many of the composition changes which have negligible influence on the energetics of the flow may be significant in controlling the electromagnetic properties of the gas. This is true for the active and passive radiative behavior ranging in wavelength from several centimeters through the ultraviolet region.

In the present work, attention is directed to the aspects of the flow which determine its response to irradiation in the regimes appropriate to communications and radar. Ionization phenomena are of particular interest here; specifically, the spatial distributions of electron density and collision frequency must be known for predicting effects in the radio-frequency bands. In cases of weak signal interactions, the determination of these quantities is a problem distinct from that of solving the equations governing transmission, reflection, and attenuation of electromagnetic waves.[1] Experimental information regarding the aerothermochemical phenomena is less extensive than that pertaining purely to the propagation of electromagnetic waves in plasmas.

Measurements of the effects brought about by ionized flows on radio propagation have been performed by means of flight tests and by laboratory simulation of certain features characterizing flight conditions. The expense and difficulty of flight tests limit the number of experiments which may be performed, thereby compromising the feasibility of exploring fully the influences of flight speed, altitude, and antenna location. As has been customary in other aerodynamic studies, these disadvantages have led to the use of laboratory

1   AF-1500-A-1

test facilities. Clearly, both types of experimentation are necessary in order to obtain a complete phenomenological picture. Laboratory propagation measurements have been reported for microwave transmission from a model in an arc-driven hypervelocity wind tunnel.[2] Interpretation of such data has been difficult because of electrode contamination of the test gas and arc interference effects on the instrumentation. Another experimental scheme is the placement of an antenna in a low-speed free jet composed of seeded combustion gases.[3] Although the flow field and gas kinetic conditions encountered in flight are not simulated in this experiment, the ionization levels can be adjusted by control of the potassium seeding. For electromagnetic properties of wakes behind high-velocity projectiles, free flight ranges[4,5] have been employed. Scaling techniques such as those given by Gibson and Marrone[6] may be extended to aid the interpretation of range results.

The use of the shock tunnel for research in nonequilibrium ionization phenomena will be discussed in this paper. For several years, shock tunnel facilities have been in use at the Cornell Aeronautical Laboratory. The development of this tool for hypersonic research has been described in some detail in a recent report by Hertzberg et al.[7] In the present work, therefore, only a brief description of the facility and instrumentation will be given (Section II). Following this descriptive section, the flow physics of the nonequilibrium phenomena governing charged particle distributions will be discussed (Section III). The effects of various ion kinetic rate processes have been studied both for flows in a shock tunnel nozzle and about a hypersonic blunt body. Regimes are delineated in which charge transfer reactions and impact ionization of molecules may be important. Other conditions are found where the simple kinetic model involving only the associative ionization ($N + O \rightleftharpoons NO^+ + e^-$) is adequate.

AF-1500-A-1

Finally, the results of recent shock tunnel experiments will be presented (Section IV). In these experiments, microwave diagnostic techniques have been employed for measuring electron densities and electron collision frequencies. The data have yielded information on the duration of useful test flow.

AF-1500-A-1

II. SHOCK TUNNEL FACILITY AND INSTRUMENTATION

A.   Description of the Facility

Basically, the shock tunnel is a short duration blowdown wind tunnel sup-
plied by gas which has been processed by shock wave compression. A nozzle
system fitted to the downstream end of a shock tube serves to expand the gas so
that stored energy is converted to directed kinetic energy. Either of two modes
of operation may be employed: a) the direct mode in which the incident shock
wave passes directly through the nozzle or b) the reflected mode in which the
stagnant gas processed by the reflected shock wave feeds the nozzle. At Cornell
Aeronautical Laboratory, the latter mode is used in conjunction with the
"tailored-interface" principle[8] in order to maximize testing time. Equilibrium
interface operation[7] is used for obtaining higher enthalpy conditions than would
be obtained with tailoring.

For the purposes of duplicating flight conditions in which ionization phe-
nomena are of interest, the shock tunnel must be designed to generate high-
enthalpy flows. Additional requirements include the ability to control the im-
purity levels in the test gas within acceptable limits and the capability of ac-
commodating relatively large-scale models in the test section. Impurities must
be held to concentrations low enough that their effect in producing or attaching
electrons is negligible compared with the ionization effects from the components
in air. Since the degrees of ionization which are significant in experiments with
radio-frequency wave propagation may be small, a high purity is sometimes a
rather stringent requirement. Large models are necessary because complete
similitude can seldom be attained for the combination of aerodynamic, nonequi-
librium, and electromagnetic phenomena. In this connection, the introduction
of the electromagnetic effects is chiefly responsible for the difficulties since the

AF-1500-A-1

simultaneous scalability of aerodynamic and nonequilibrium effects has been theoretically demonstrated[6,9,10] for a wide range of condition. The additional requirements for electromagnetic similitude in hypersonic flows have been discussed in a previous paper.[1]

In an effort to meet the requirements touched upon in the preceding paragraph, a six-foot hypersonic shock tunnel has been developed at Cornell Aeronautical Laboratory. Figure 1 illustrates the physical layout of the tunnel. The driver tube is equipped with a heating jacket and is designed for the use of hydrogen at temperatures up to 750°F at a pressure of 2000 atm. This tube is 14 feet long and has an inside diameter of 4.75 inches. The driven tube, which is 28 feet in length and 3.00-inch inside diameter, is connected to a multi-stage nozzle system. Figure 2 shows a detailed view of the nozzle system in partial section. The two-dimensional expansion contour of the primary nozzle is designed for wave cancellation in equilibrium airflow. The equilibrium Mach number at the exit of this nozzle is approximately 4.5. The throat area of the primary nozzle is chosen so that the exhaustion of the reservoir test gas as determined by the quasi-steady mass flow rate occurs at the time of arrival of the first expansion wave from the driver at the nozzle entrance. A 10° flow turning section removes solid particles from the air stream by centrifugal action and bleeds the boundary layers. The final stage is a conical nozzle (10° - half angle) in which the flow expands to the six-foot test section and receiver vessel shown in the foreground of Fig. 1. Interchangeable liners for the primary nozzle and entrance lips for the terminal nozzle provide means for varying the test Mach number range. The conical portion between the one-foot diameter station and the six-foot test section is made of bonded glass fiber having a thickness for optimal transmission of X-band microwave radiation at 9396 Mc/sec.

B.   Tunnel Performance

Figure 3 shows the range of flight duplication conditions theoretically accessible with the tunnel. The altitude-speed characteristics are particularly well suited for the study of flow conditions about re-entering satellites and boost-glide vehicles.

The measured performance of the shock tube using heated hydrogen as the driver gas and air as the test gas is shown in Fig. 4 and represents the current high-performance limit. This figure shows a plot of stagnation enthalpy and reflected-to-driver pressure ratios versus shock Mach number. The thermodynamic state of the gas in this reflected shock region is determined from measurements of the incident shock velocity and the stagnation pressure. It has been found that for shock tube operation near the tailored-operating point that the waves generated due to the mismatch are quickly attenuated so that a steady reservoir condition is in fact attained. As the waves generated are very weak, the final state is determined by assuming an isentropic process to occur from the region behind the first reflected shock to the final steady state condition. In order to obtain a sufficient duration of uniform reservoir conditions, the shock tube is operated near the tailored-interface conditions. Contamination of the test gas by mixing with the driver gas is minimized by operation under conditions where the interface separating the driver and driven gases is stable. In this context, stability refers to that condition where the density of the hydrogen gas is less than that of the shocked air at the interface zone so that any mixing due to instabilities does not contaminate the region of the nozzle inlet.

Calibration studies of the nozzle-test section system have included pitot pressure surveys across the tunnel using a multiple-probe rake. The pitot pressure distributions at the test section for a range of reservoir conditions

are shown in Fig. 5. These data were taken with the 2-5/8" inlet diameter of the second-stage nozzle.

Information on flow angularity with respect to the 10° nozzle axis has been obtained from the results of heat transfer studies on a slender cone[11] following techniques described in Ref. 12. The results of these tests indicate the centerline flow at the test section station to have a total angularity of less than 1°.

C. Instrumentation

Methods for the accurate collection of data under conditions of high velocity, high temperature, and short test flow duration are necessary in shock tunnel research. Cathode-ray oscilloscopes provide adequate means of recording pressure and heat transfer information. Rapid response instrumentation for measuring the wide range of pressures encountered in shock tunnel research includes modified microphones and a variety of piezoelectric crystal transducers.[7] The design of the transducer porting incorporates shielding from the thermal radiation of the gas flow in such a way that excessive blockage does not seriously increase the over-all response time. Transient surface temperatures are measured with thin-film resistance thermometers mounted on dielectric backing material.[13] Specifically, the gauges consist of platinum films of the order of 1000 Å thick painted or sputtered on a Pyrex backing block. Heat fluxes are recorded directly from an analogue network[14] which receives the temperature signal from the thermometer. A pulse method[15] is employed for determining the thermal properties of the backing material. Thin insulative coatings are applied to the outer surface of the thin film in order to block any electrical conduction paths through the ionized gas flowing over the surface.[16] Detailed discussions of the theory and application of the aerodynamic instrumentation may be found in Ref. 7.

AF-1500-A-1

The thin-film gauges have been found to respond to microwave radiation as well as aerodynamic heat transfer. In order to separate the two effects, gauges are mounted both on the exterior and interior surfaces of the model, and the wall of the model is designed for microwave transparency. Glick[17] has investigated the microwave response of these gauges theoretically and experimentally. A heat transfer analysis was carried out for a two-layer slab; the first layer is assumed to be bounded on one side by an adiabatic surface and on the other by the interface with the second layer which is assumed to be semi-infinite. Uniform volumetric heat generation is specified for the first layer. Solutions of the heat equations and substitution of the properties of the thin platinum film and the Pyrex backing show that the temperature in the film is essentially uniform for times greater than 10^{-6} seconds. For these times, the temperature time variation of the film approaches that at the surface of a semi-infinite homogeneous solid with constant heat input equal to the energy generation in the gauge per unit area of film surface. The antenna characteristics of the gauge and its equivalent circuitry were also analyzed in Ref. 17. It was found that the generation term was directly proportional to the electromagnetic energy flux. The proportionality factor can be determined theoretically on the basis of the analytical results. An experiment was performed to determine the dependence of equivalent heat flux on the angle between the electric field direction and the dipole direction characterizing the gauge if it were considered to be an antenna. The results verified the fact that the gauge acts as a dipole antenna rather than a simple absorber, which would not exhibit any angular dependence. In Ref. 17 an example is given for a platinum thin-film bolometer of thickness 10^{-7} meters and length of about 3×10^{-3} meters. The useful range of this gauge as a bolometer is estimated to be 0.025 to 23 watts/cm^2 of incident microwave radiation flux.

The electronic components used for both aerodynamic and microwave instrumentation are standard for the most part, and will be described diagrammatically in the context of the experimental discussion.

AF-1500-A-1

III. THEORETICAL STUDIES OF NONEQUILIBRIUM PHENOMENA

A. Delineation of Problems

Some of the most important features in the interpretation of data obtained in high-enthalpy shock tunnel research involve nonequilibrium phenomena. Because of the large degrees of dissociation and ionization initially existing in the test gas before expansion, the aerothermochemistry of the nozzle flow must be analyzed in order to determine conditions in the test section of the tunnel. Furthermore, certain aspects of the hypersonic flow about a model (or a flight vehicle) are dominated by nonequilibrium effects. In the present work the influence of coupled rate processes on the distributions of charged particles will be emphasized because the chemical aspects of the problem have been discussed in detail in previous papers (e.g., Ref. 10). Kinetic mechanisms of varying degrees of complexity will be examined in Subsection B in order to evaluate existing simplifications and their effects on electron distributions in particular. After the computational models are established, results from the various models will be compared in Subsection C for nozzle flows at conditions appropriate to shock tunnel testing. In Subsection D, the ionization histories will be examined for the stagnation streamtube in a hypersonic blunt-body flow for various kinetic models.

B. Basis of Ionization Kinetic Models

In most of the hypersonic flow conditions considered here, the rate processes involving the neutral particles dominates the thermodynamic history of a fluid element and the ion kinetics are governed by this history. The neutral

AF-1500-A-1

particle reaction model employed in Ref. 10 is used for all cases (see Table I).
The use of this set of reactions is fully discussed in Ref. 10.

A major portion of previous work on nonequilibrium ionization in air has
been limited to associative ionization (and the reverse, dissociative recombi-
nation) types of reactions because these are energetically favored. Exceptions
to this include Refs. 18 and 19. In Ref. 18 two charge transfer reactions were
added in shock wave calculations and in Ref. 19 the added effects of atomic ions
governed only by three-body Thomson recombination were examined in expansion
calculations. Both additional effects are studied simultaneously in this paper.
For shock tunnel expansions from relatively high-pressure reservoir conditions,
the negative oxygen atomic ion is added in one case to determine its effect on
test flow electron concentrations. When O^- is included, collisional detachment
and mutual neutralization reactions are included. Radiative and dielectronic
recombination processes are omitted for the reasons given in Ref. 19; i.e.,
faster competitive recombination paths exist for the range of conditions chosen.

Table 2 summarizes the ionization reactions and the corresponding rate
constants which have been employed in the present studies. Reactions 10-12
are dissociative recombination of NO^+, N_2^+ and O_2^+ respectively with elec-
trons. Reactions 13-22, 40-49 are three-body recombinations, reactions 23-
33 are charge transfers, reactions 34-38 are mutual neutralizations, and re-
action 39 is three-body attachment. The rate constant used for reaction 10
is that obtained experimentally by Lin[20] and reported in Ref. 18. Axial micro-
wave reflection experiments[21] carried out in a shock tube at CAL yield values
for ionization relaxation distance of the same magnitude as that predicted from
rate data given in the earlier work cited. Theoretical calculations of the cross
section have also been reported recently.[22] The value obtained for 1 ev.

electrons is an order of magnitude greater than that given in Ref. 18. It should be pointed out that the theoretical estimate is for monoenergetic electrons, and is, therefore, not specifically comparable with experimental results for thermalized electrons. Microwave phase-shift measurements of ionization in a nozzle flow are being employed at the time of this writing to determine the rate constant for reaction 10. Early indications are that k_{10} is the same order of magnitude as the value listed in Table 2. This shock tunnel nozzle experiment and its theoretical interpretation are the subjects of Section IV of this paper. Rate constants for reactions 11 and 12 are based on theoretical estimates given in Ref. 18. Reactions 13-22 and 40-49 are three-body Thomson recombination reactions. The rate data for these reactions were computed theoretically according to the classical Thomson theory modified where necessary for inelastic collisions of electrons with molecules. The inelasticity factors were taken to be constant and were obtained by averaging over the energy range of interest.

Electron-ion recombination reactions (10-22) constitute parallel paths for electron removal which are coupled only through the electron concentration. Over most of the density range of interest in hypersonic flight and in shock tunnel operation, the binary reactions (10-12) are by far the most active paths in electron removal and their reverse reactions likewise are the most significant in electron production. The atomic ions may be neutralized relatively efficiently by means of charge transfer processes of the types

$$A^+ + BC \rightleftharpoons AB^+ + C$$

$$A^+ + BC \rightleftharpoons A + BC^+$$
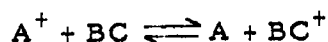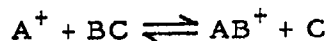
which are required for completion of the coupling through atomic ions. A, B, and C are symbols, any of which may be N or O. These classes of reaction produce diatomic ions, which have a much higher probability of reaction with

electrons than the atomic ions because of the dissociative processes. As brought out in the classical chain reaction theory of chemical kinetics, certain chain carriers may have a strong influence on over-all kinetics despite their relatively small equilibrium, or quasi-stationary concentration. For this reason, the effect of charge exchange reactions on electron densities will be considered in the present work. Although experimental rate data are unavailable for the charge transfer reactions in the temperature range of interest here, conservative estimates have been employed. The rate constants for reactions 23-33 are those given in Ref. 18 which are based on the assumption of cross sections of order πa_o^2 for all charge transfer reactions (hence the $T^{1/2}$ dependence). a_o is the first Bohr radius. Such an assumption is reported to agree[18] with unpublished experimental data for reaction 25.

The theory of Eyring, Hirschfelder, and Taylor[23] gives a reaction cross section inversely proportional to the relative speed of collision partners so that the rate constant would be independent of temperature. This theory was developed for particles which obey a Maxwellian velocity distribution and which have no permanent dipole moment. The energy of activation is considered to be that at the maximum in a surface defined by the difference between the rotational energy of the colliders and the polarization energy of the encounter. The rate constant is determined to a constant κ (a transmission coefficient) by carrying out the collision integral to determine the rate of passage over the barrier in the energy surface. For a transmission coefficient of unity, the expression for the rate constant is as follows

$$ k = 2\pi \left(\frac{\alpha e^2}{\mu} \right)^{1/2} $$

where α is the polarizability, e the electronic charge and μ the reduced mass of the colliding pair. Table 3 summarizes the polarizability data used

and the rate constants obtained with the theory of Ref. 23. Reactions 26, 27, 31, and 32 are omitted because nitric oxide has an electric dipole moment, $\mathscr{q}$, of 1.6×10^{-19} esu, and the theory of Ref. 23 is not strictly applicable. An estimate for the polarizability may be obtained by using the formula developed in Ref. 24, $\alpha = \alpha_0 + (\mathscr{q}^2/3kT)$ with α_0 as determined in Ref. 25 (1.68×10^{-24} cm^3). At 6000°K the permanent moment contribution given by this formula is of the order of 1% of the induced moment because of thermal randomization. Hence, $\alpha \approx \alpha_0$, and the charge transfer rate constants for reactions 26, 27, 31, and 32 may be expected to be of the same order as the others in the limit of this approximation.

Numerical estimates of the charge transfer rate constants have also been given by Beran[26] for 5000 to 6000°K and by Meyerott,[27] Krasovskii,[28] and Nawrocki[29] for upper atmospheric conditions (presumably several hundred °K). The various estimates based on theory and observation are spotted on a graph of rate constant vs temperature in Fig. 6. Note that the line based on the πa_0^2 cross section is conservative compared with all other estimates except that of Ref. 29. Nawrocki gives rather wide uncertainty margins ($\log_{10}k = 11 \pm 1$).[29] Therefore, this source may be weighted less than the others. The use of conservative estimates of k_{23-33} will minimize the effects which they have on the system. This procedure is necessary because of the uncertainties in the rate constants.

In the density regimes encountered at the early portion of nozzle expansions typical of shock tunnel testing, significant amounts of O^- might be expected because oxygen atoms are abundant and have relatively high electron affinity (1.46 ev). Either the affinities of the other species present are much smaller than that of the oxygen atom or the neutral species in question are

present in much lower concentration. Therefore, all other negative ions are neglected in this work. The reactions involving this species are Nos. 34-39 in Table 2. All but the last reaction of this group are mutual neutralizations. Since the interaction is governed by the long-range coulombic potential and the excess energy may be carried off by recoil (as well as excitation), mutual neutralization is an extremely efficient type of reaction. Reaction 39 is a three-body attachment where M represents any third body. This reaction is a close analogue to three-body neutral atom recombination - in fact its rate constant at $300^\circ K$ is of the same order of magnitude as that for the corresponding reaction involving neutral species. Dissociative attachment to O_2 and NO are omitted because these reactions have moderate activation energies. Hence, their rates would vanish exponentially with decreasing temperature. Rate constants suggested in Ref. 29 were employed for reactions 34, 36, and 39. The negative one-half power temperature dependence for reactions 34-38 (inclusive) was also given in Ref. 29. Rate data for reaction 35 were obtained from Massey's article[30] on gaseous ion recombination, and those for reactions 37 and 38, from Mitra.[31]

For ease in future reference, the various reaction kinetic models will be numbered as follows:

Model Number	Species[*]	Reactions[*]	Remarks
1	1 - 8	1 - 10	Basic model ($NO^+ + e^- \rightleftharpoons N + O$)
2	1 - 12	1 - 22	Add three-body recombination of atomic ions
3	1 - 12	1 - 32	Add charge transfer
4	1 - 12	1 - 33	Add charge transfer
5	1 - 13	1 - 39	Add mutual neutralization and attachment
6	1 - 12	1 - 22, 40 - 49	40 - 49 are three-body recombination involving molecular ions
7	1 - 12	1 - 12, 23 - 33, 40 - 49 15 - 17, 20 - 22	

C. Shock Tunnel Nozzle Flows

At the shock tunnel condition considered here, ($T_o = 8000°K$, $p_o = 100$ atm), the variation of aerothermodynamic quantities (p, ρ, T, u, and M) are principally controlled by the interaction of the coupled chemistry of the neutral species with the dynamics of the expansion process. The method of computation and the first results for hypersonic nozzle airflow governed by coupled chemical reactions appear in Ref. 32. Further analysis and discussion of these results in the context of hypersonic tunnel testing appear in Ref. 10. In the rapid expansion of the high-enthalpy flow through a shock tunnel nozzle, various chemical degrees of freedom may exhibit nonequilibrium lags because molecular collisions become less and less frequent. Although vibrational lag processes are believed

---

[*] Species and reaction numbers are given in Table 2.

to have little effect on the gasdynamical history, [10] the freezing of various chemical processes can withhold rather large fractions of energy from the flow. Rotational and translational relaxation, being relatively efficient processes, can safely be considered to equilibrate throughout the entire expansion history. The fraction of oxygen atoms tends to become constant rather early because the ternary recombination reactions freeze first and no efficient binary paths exist for removing oxygen atoms. On the other hand, nitrogen dissociation is substantially equilibrated when sufficient nitric oxide is present to participate in the fast binary reactions (8 and 9) which remain active after the ternary reactions (1 - 7B) freeze.

Nitric oxide molecules undershoot the equilibrium curve when insufficient O_2 is present to replenish NO through reaction 8 as NO is consumed by reaction 9. If nitric oxide is seriously depleted, the nitrogen atom fraction suddenly halts its descent. Otherwise, it levels out gradually as the two-body reactions become ineffectual. The chemical composition histories for the shock tunnel cases considered for the ionization studies is shown in Fig. 7. [32] The nitrogen atom concentration drops until the exchange reactions freeze in the region of NO-undershoot.

As shown in Ref. 32, collision frequency of N-atoms with O_2 and NO is sufficiently high at p_o = 1000 atm to equilibrate nitrogen dissociation throughout. Table 4 summarizes the gasdynamic consequences of chemical nonequilibrium. [32] For more complete discussion of the behavior of neutral particles, the reader should consult Refs. 10 and 32.

Previous work on nonequilibrium ionization in expanding air flows appears in Refs. 19 and 33. Ion kinetic model 1 with the addition of Thomson recombination of $(e^- + NO^+)$ is the basis of approximate freezing solutions [33] utilizing

17   AF-1500-A-1

a freezing criterion. Electromagnetic wave penetration depths in the test flow of the CAL six-foot tunnel are also shown in Ref. 33. Two conclusions are apparent from these results: (1) Thomson three-body recombination is comparable with dissociative recombination in air only at the highest reservoir density considered ($\rho / \rho_{std} \sim 75$) and, (2) the flow in the test section of the tunnel should be expected to be transparent to UHF and microwave radiation. As will be described in a later section, this conclusion has been borne out experimentally.

The more recent work on ionization nonequilibrium in airflows is covered in Ref. 19. Exact solutions are compared with approximate solutions and it is shown that for certain flow conditions, the electron fraction does not approach a constant value asymptotically, but rather decreases as some power of distance dependent upon frozen chemical composition and nozzle geometry. For completely frozen ionization, the d.c. conductivity reversal is demonstrated for pure and for cesium-seeded airflows. Ion kinetic model 1 was employed for the nozzle flow solutions in Ref. 19.

In the present work, ion kinetic models 1, 3 and 5 will be compared for the reservoir state of ($T_o = 8000°K$, $p_o = 100$ atm). Model 1 consists only of the fastest electron removal mechanism because electrons are completely counterbalanced by diatomic ions capable of reacting in two-body recombinations, whereas in model 3, the electrons have positively charged counterparts made up of both atomic and molecular ions. If the removal of atomic ions were solely dependent on reactions with electrons (such as in model 2), the ionization system would freeze suddenly as soon as the supply of molecular ions was depleted by dissociative recombinations. This behavior would bear a close resemblance to that of nitrogen dissociation freezing, which occurs in airflows when the number

of nitric oxide molecules diminishes sharply. In model 3, however, reaction paths (23-33) other than three-body recombination (13-22) are allowed for the removal of the atomic ions.

In reactions 23-33, atomic ions may be neutralized by acquiring an electron from some previously neutral collision partner. If the collision partner is diatomic, the positive ion formed may then participate in binary recombination with electrons. The supply of diatomic ions depends on a balance set up between production by charge transfer and consumption by recombination. Thus, molecular ions are truly chain carriers in the neutralization of atomic ions when charge transfer occurs. After the rates of endothermic reactions become relatively small, the chains are of the forms:

$$A^+ + BC \longrightarrow C + AB^+$$

$$AB^+ + e- \longrightarrow A + B$$

and

$$A^+ + BC \longrightarrow A + BC^+$$

$$BC^+ + e^- \longrightarrow B + C$$
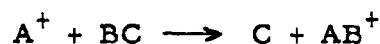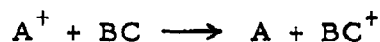
These chains remain effective after the Thomson processes

$$M + A^+ + e^- \longrightarrow A + M$$
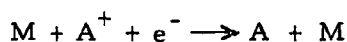
has effectively vanished in the expanding flow.

The detailed chain structure may be represented by the parallel heirarchy of exothermic reactions shown in Fig. 8. From an energetic point of view, N_2^+ seems to be an exception to this rule. Reactions 23 and 28 are exothermic to the right by 2.0 and 1.0 e.v. respectively. The forward activation energies are zero; therefore, the reverse reactions freeze more rapidly in an expanding flow because of the exponential dependence of the reverse rate on temperature. In

departures from ionization equilibrium then, the net result of reactions 23 and 28 is to oppose the chain for removing atomic ions, and the atomic ions themselves are chain carriers in a series of reactions for N_2^+ removal in competition with reaction 12.

With the additional species and reactions in model 3 as compared with model 1, two alternative questions are answered by carrying out exact solutions: 1. Are charge transfer reactions (24-27; 29-32) rapid enough to impart to the ionization system the gross behavior of binary recombination, or 2. Are charge transfer reactions 23 and 28 sufficiently influential to oppose the electron removal chain by producing O^+ and N^+ at a rate exceeding removal by reactions (13-22; 24-27; 29-32).

Figure 9 shows the ionization history in the nonequilibrium nozzle flow considered. Kinetic models 1, 3, and 5 have been compared. The electron concentration histories for models 1 and 3 practically coincide (particularly at large area ratios). This shows that at an early stage the charge transfer reactions effectively eliminate all atomic ions which initially counterbalance 4.3% of the electron population. If these fast chain reactions were not considered, the atomic ions would recombine only by the paths set out in reactions 13-22 which freeze relatively earlier because of higher order density dependence. Model 5 contains O^- as an additional species along with six reactions. At the stagnant reservoir conditions, negative oxygen ions are about 1/20th as numerous as electrons. During the expansion, however, the mutual neutralization reactions (34-38) prevent freezing of O^- which would occur rather early if reverse reaction 39 (collisional detachment) were the only removal process in operation. This ratio is maintained or slightly reduced in the expansion. Compared with the case without O^-, the electron population is reduced by less than 5%.

From these comparisons it may be concluded that the simple ionization kinetics represented by model 1 are adequate for predicting ionization levels in shock tunnel test flows for stagnation temperatures up to 8000°K and at pressures where nonequilibrium effects are significant. Since conservative estimates have been employed for the charge transfer cross-section, this conclusion may well hold above the temperature considered here. At temperatures lower than 8000°K, positive ions other than NO^+ are not significant. Clearly, at some high temperature, molecular ions will not be numerous enough to maintain any of the fast chains involving charge transfer or dissociative recombination, and freezing of the ionization may occur very early.

D.   Inviscid Hypersonic Flow About a Blunt Body

The significant chemical features of these flows were discussed in Ref. 10 principally for processes controlling the distribution of energy among the various degrees of freedom. Since the present work is mainly concerned with the plasma kinetics of the flow, only a brief summary of the neutral particle aerothermochemistry will be given here. Clearly, viscous effects will play an important role in the flow near the body surface. However, the purpose of the present work is the assessment of ionization kinetic mechanisms and their effects on the plasma properties. For this purpose, inviscid solutions are adequate for providing the thermodynamic environment typifying high altitude hypersonic flight.

1.   Review of Neutral Particle Effects

The initial effect on a fluid element as it is processed by the detached shock wave preceding a blunt body is rapid excitation of translational degrees of freedom. Practically coincident with this process is rotational excitation. At many flight conditions typifying re-entry trajectories, vibrational and

dissociational relaxation are interdependent through a complex coupling mechanism.[10] As the molecules in air dissociate to form atoms, nitric oxide is formed by rapid atom exchange reactions. These reactions approach quasi-equilibrium so rapidly that the nitric oxide concentration overshoots infinite rate equilibrium values; this occurs to a great degree along the higher entropy stream surfaces emanating from the central portion of the shock wave. As the gas expands and accelerates in the flow about the body, the temperature and density decrease, driving downward the local equilibrium atom-concentrations. The presence of nitric oxide in significant concentrations favors the removal of nitrogen atoms through rapid, two-body paths; on the other hand, oxygen atomic recombination freezes early. When the reaction of N with NO dissipates the supply of nitric oxide more rapidly than the $N + O_2$ reaction (8) replenishes it, nitrogen atom recombination freezes and nitric oxide undershoots equilibrium. Except for altitudes of 100 Kft and below, nitric oxide becomes depleted so rapidly that the nitrogen-atom fraction changes very little from its stagnation level in the flow near the surface of typical re-entry vehicles. In outer streamlines, freezing may occur before dissociation is complete because of the high velocity and rapid expansion immediately behind the shock.[6,10]

These features of nonequilibrium airflows about blunt hypersonic bodies have been brought out in numerical solutions obtained by means of computing machine codes. The roles of the endothermic processes in the shock wave detachment region about the nose cap have been investigated by the inverse method which has been extended[34] to coupled nonequilibrium flows. The results of this work were described in a brief paper.[35] In addition to the series of reports under Ref. 34, detailed results and discussions of nonequilibrium behavior are found in Ref. 10. The expansion freezing behavior in the streamtubes originating

AF-1500-A-1

from the stagnation equilibrium region has been studied by means of an adaptation[10, 32] of the nozzle flow code to prescribed pressure distributions.

In the present work, the ionization kinetics are studied for one flight condition typical of a ballistic re-entry vehicle (speed = 23 Kft/sec, altitude = 150 Kft) and one flight condition typical of a lunar probe re-entry vehicle (speed = 36 Kft/sec, altitude = 200 Kft). For illustrative purposes, flow field solutions are limited to a stagnation streamline starting from the detached shock, going centrally inward to the stagnation point, and proceeding around the body at the surface. The body chosen is a hemisphere-cylinder with a 1-foot nose radius flying at zero yaw. In the ballistic re-entry condition the energy residing in ionization is small compared with the total enthalpy; however, in the lunar probe re-entry condition nearly 18% of the energy is in ionization. For the decelerating portion of the streamtube flow between the shock wave and the stagnation point, the normal shock wave numerical code[34] was used with a streamwise coordinate transformation[6] to adapt the parallel flow case to the stagnation point flow. For the accelerating flow from the stagnation point around the nose and along the afterbody, an adaptation of the nozzle flow numerical code[32] was used. Modified Newtonian and blast wave pressure distributions were assumed for the nose cap and afterbody respectively as described in Ref. 10.

2.   Ballistic Re-entry Case

Three cases are compared for the ionization in the flow about a ballistic re-entry vehicle.

Case A[*] consists of reaction kinetic model number 1 for the entire flow. This is included for comparative purposes because much of the previous literature on air ionization is limited to such a mechanism.

_____

[*]   Cases A and B were previously shown in Ref. 19.

Case B* is based on model 6 for the decelerating flow and on model 2 for the accelerating flow. In these models, all of the singly positive ions are included as well as electrons. Model 6 differs from model 2 in that it allows impact ionization of diatomic species. The reverse reaction, three-body recombination of electrons with positive diatomic ions, is overshadowed by dissociative recombination in the exothermically lagging condition in expanding flow; hence, the choice of model 2 for that flow. Early in the history of the shock wave relaxation zone, atoms are not yet produced in large quantities and translational energy is large. Although the probability of dissociation is much higher than that for ionization, it is interesting to compare the impact ionization rate with the associative ionization rate in the early stages.

Case C includes the addition of the charge transfer reactions to Case B. Model 7 is employed for the decelerating flow and model 4 for the accelerating flow. Models 4 and 7 differ in the same way as models 2 and 6. For the afterbody flow an incidental comparison is made in Case C between models 4 and 3; i.e., the omission of the $N^+ + O$ charge transfer reaction is considered.

Figure 10 shows the ionization histories along the stream surface passing through the stagnationpoint for Cases A, B, and C relating to ballistic re-entry conditions. Case A exhibits the familiar overshoot of electron concentration causes by the $N + O$ associative ionization reaction seeking a local equilibrium level higher than the final level. Characteristically, there is little change from the stagnation region to the sonic point. However, the dissociative recombination is rapid enough to follow the rapidly decreasing local equilibrium in the supersonic

region for a considerable distance. The change in slope in the shoulder region is caused by the difference between the decay rates of the Newtonian and blast wave pressure distributions assumed. It was brought out in Ref. 19 that the nonequilibrium electron concentrations undershoot the infinite-rate equilibrium curve.

Case B exhibits two rather distinct regimes in the shock wave relaxation zone. The early portion, at low ionization levels, is controlled by impact ionization and the final rise, by associative ionization. It should be observed here that the rates of ionization are calculated through the equilibrium constant by means of the recombination rate constant and the assumption of detailed balancing. The particular reactions governing the early portion of the rise have recombination rate constants which are considerably enlarged by inelasticity factors.[19] The argument for using such factors is based on the ability of molecular colliders to absorb energy in internal modes,[36] thereby enhancing greatly the probability of recombination. The reverse argument for the ionization rates must, therefore, be based on the possibility of a vibrationally excited molecule contributing its internal energy to help ionize a collision partner. The result shown in Fig. 10 is based on the assumption of vibrational equilibration throughout, and must be regarded as an upper limit for the effect of the additional reactions. Evidently, this is not as bad an assumption as it may seem because fast vibrational excitation paths are available through the exchange reactions which are frequent at these temperatures.[37] The coupling of dissociation with vibration as discussed by Treanor and Marrone[38] is not significant in the region under consideration here.

The continuation of Case B through the overshoot region and back to the sonic line does not show significant variance with the qualitative behavior of

Case A. Levels are elevated by some 30% because of the inclusion of additional ions. The minimum in the curve for Case B indicates a delay in the ionization of atomic species which is allowed to occur only by impact with this model. Beyond the sonic line, the curve for Case B differs markedly from that for Case A. Since atomic ions can recombine only through three-body paths, all of the atomic ions are frozen at essentially stagnation levels. This is typical of ternary reactions for the flight conditions considered. Thus, when all of the molecular ions are neutralized, the remaining electrons freeze at a concentration approximately equal to the sum of the stagnation levels for both atomic ions.

Case C is practically identical to Case B throughout the decelerating flow region. The charge transfer reactions provide a more efficient means of producing atomic ions downstream from the overshoot peak. For this reason, the dip in the curve preceding the stagnation point is not as pronounced as it is with Case B. Downstream from the sonic line, Case C more nearly resembles Case A than it does Case B. The atomic ions are neutralized by receiving electrons from neutral molecules through the charge transfer reactions. The reaction chains shown in Fig. 8 govern the system, and the molecular ions recombine with electrons through fast, dissociative reactions. This drives the electron concentration below that in Case A because the local equilibrium ionization levels are actually depressed in the afterbody region by the inclusion of the additional ions. The key to this phenomena lies mainly in the depression of NO^+ concentrations at stagnation conditions. Because nitric oxide has an ionization potential considerably below those of the other species and because there is less nitric oxide present, the local equilibrium ionization curve (which is essentially determined by nonequilibrium behavior of the neutral species which are not shown) is steeper in the far supersonic portion of the expanding flow. ..

AF-1500-A-1

The omission of reaction 33 which cross-links the chains shown in Fig. 8 has practically no effect at the conditions of Fig. 10. At higher altitudes this omission leads to sudden freezing of N^+ because the $N + N_2^+$ charge transfer reaction (28) produces N^+ at a greater rate. This arises from higher initial levels of N-atoms and earlier freezing of N-atoms. In the cases studied, initial N^+-concentrations are higher also. The sudden freezing then is caused by the establishment of a quasi-stationary N^+-condition in the left-hand branch of the charge transfer mechanism shown in Fig. 8.

It has been demonstrated by these comparisons that for ballistic re-entry conditions, levels and gradients of electron density are sensitive to the choice of reaction mechanism in certain regimes. The reflection of electromagnetic waves from a nonuniform plasma has been shown[1,21] to be highly dependent upon both these features. Therefore, when electromagnetic propagation problems are considered, it would appear that the same care must be taken in selecting an ionization mechanism as has been taken in the chemical case. The impact ionization reactions may play an important role in the early part of the shock wave relaxation zone, and the charge transfer reactions are significant in the afterbody nonequilibrium flow. Of course, the associative ionization reactions and their reverse reactions are basic to any kinetic scheme for ionized species. It will be recalled that at pressures appropriate to shock tunnel operation, the charge transfer reactions eliminate atomic ions early in the expansion. The remaining portion of the ionization history is, therefore, governed by the simple model 1.

3.   Lunar Probe Re-entry Case

The ionization history for a lunar probe re-entry flow field at 200 Kft in altitude is dominated by atomic ions. Therefore, the complexities of model 7

27   AF-1500-A-1

must be included until some rational simplifications are discovered. Figure 11 shows the positive-ion distributions as well as the electron distribution for such a case. The molecular ion concentrations display large overshoots in the very early part of the shock wave relaxation zone. This occurs as the associative and collisional ionization mechanisms are opposed by the charge transfer reactions which give rise to the atomic ions. Note that the electron concentration distribution has two regimes; one corresponds to the formation of molecular ions and the other, to the formation of atomic ions. This explanation differs from that given for the ballistic re-entry case which is dominated throughout by molecular ion formation following two different mechanisms successively. In the afterbody flow, the atomic ions freeze leading to a complete freezing of ionization at a relatively higher level than that in the 23 Kft/sec case. The deionization chains shown in Fig. 8 depend on the presence of neutral molecules to a great extent. If concentrations of these species go below a certain level, and molecular ion concentrations are low, the reaction chains do not function. Note the decrease in N^+ concentration and the increase of the O^+ concentration to the final levels. This occurs because of the different behavior of the local equilibrium trends and the ultimate freezing of the charge transfer reactions.

Other information relating to the flow field is given in Figs. 12, 13, and 14. Neutral particle histories shown in Fig. 12 qualitatively resemble those obtained for lower energy re-entry conditions. Molecule concentrations are generally much lower, except nitric oxide overshoots the stagnation equilibrium level by a considerably greater amount. Temperature and fluid density distributions are shown in Figs. 13 and 14 respectively since these are quantities of interest in plasma and radiation calculations.

AF-1500-A-1

E.   Summary of Nonequilibrium Theoretical Results

The establishment of further generalization in ion kinetic models has revealed regimes of practical interest in which the single nitric oxide ionization model may not be sufficient for describing the electron density distributions in nonequilibrium airflows. For nozzle flows appropriate to high-enthalpy aerodynamic studies at reservoir stagnation temperatures up to 8000°K, the simple model appears to be adequate. However, in the early part of the relaxation zone behind the strong portions of a detached shock wave at ballistic re-entry conditions, impact ionization of molecules may be significant. In the afterbody and wake flows, charge transfer processes contribute to the deionization mechanism. For superorbital re-entry flow, a complex kinetic model may be necessary because of the dominant role of atomic ions.

The present work must be regarded primarily as an heuristic enterprise at the present time because of important unanswered questions in high-temperature gas kinetics. Ionization of electronically excited species and excitation kinetics have not been included. Vibrational-rotational coupling with one another and with dissociation has been omitted. Radiative coupling and photo-processes have not been considered in the analysis. Enhancement of three-body processes due to electrons as catalytic bodies has not been accounted for. Further experimental research guided by theory must be undertaken not only to improve the data for the processes included, but also to permit the rational consideration of the additional effects enumerated above.

IV. IONIZATION EXPERIMENTS IN THE SHOCK TUNNEL

The theoretical results given in the previous section indicate the necessity of rather complex ion-kinetic models for certain re-entry body flow conditions. However, they further show that model 1 (species 1-8, reactions 1-10) is adequate for describing nonequilibrium ionization in shock tunnel flows of current interest. In effect, the electron density at moderate-to-large area ratios is determined only by reaction 10 because efficient removal processes quickly eliminate all ions except NO^+ and e^-. The present experimental program is being pursued in an effort to determine the rate constant for reaction 10. Previous experimental studies of reaction 10 by other methods have been discussed in Section III, Part B. A second objective of the experiment was the study of the gasdynamic processes determining the duration of useful test flow in the tunnel. Phase shift measurements obtained with an X-band (9397 Mc) microwave interferometer were employed to obtain electron density levels at the 2.6-inch entrance to the terminal (conical) stage of the nozzle system (Fig. 2). Pitot pressure measurements were obtained simultaneously in the six-foot test section in an effort to correlate the sequence of events involved in starting the nozzle with the ionization histories. One advantage of a nozzle kinetic experiment is the removal of spatial resolution difficulties which may be encountered in shock wave relaxation zone experiments.[20,21]

A. Microwave Interferometer

The microwave interferometer was used to measure the phase shift of electromagnetic waves due to propagation through the plasma, which acts as a dielectric medium. This technique has been widely applied in gaseous discharge research and has been described fully in the literature relating to that field

(e.g. Refs. 39 and 40). Microwave diagnostic methods are analogous to optical probes in that the propagating signal is so weak that it leaves the test gas essentially undisturbed.

Figure 15 shows a schematic diagram of the bridge circuit of which the interferometer is comprised. Power is supplied by a klystron oscillator through an isolator in order to prevent reflected power from entering the oscillator. A directional coupler is employed to divide the power between the test arm and the reference arm. Cross-guide couplers with crystal detectors are mounted on either side of the test region in order to measure reflected and transmitted power. Horns are used to obtain transmission through the plasma. The reference arm is equipped with a phase-shifter and an attenuator which are used both to initially balance the bridge and to quantitatively measure the unbalance produced by the plasma. A detector is used to monitor power level in the reference arm. A magic-tee is used to mix the power from the two arms. The mixed signal is fed to the final detector through an isolator. Thus, the detected mixed signal is affected by attenuation and phase-shift in the plasma.

Figure 16 shows the physical arrangement and location of the microwave circuitry. The transmitted signal is directed normal to flow direction through windows made of bonded glass fiber. The thickness of the windows was selected for optimal transmission of X-band (9397 Mc) microwave radiation. The test signal passes through the plasma in a region immediately downstream from an expansion fan which turns the flow through 10^ϵ and upstream from the entrance lips to the conical nozzle. Turning the flow centrifuges out any solid material. Therefore, the flow is gasdynamically uniform with the exception of the boundary layers on the windows. Boundary-layer growth in the primary nozzle was computed (for the range of conditions used) by means of an empirical relationship given in Ref. 41. The displacement thickness of the boundary layer on the

31   AF-1500-A-1

Fiberglas windows was approximately 0.4 of a free-space wavelength at 75 atm reservoir pressure and decreased to 0.15 at 680 atm while the total path length through the plasma is about four free-space wavelengths at X-band.

The first step in calibrating the interferometer is tuning out the mismatch between the horns with no plasma present. This is necessary because multiple reflections between the horns give rise to a standing wave. It is difficult to maintain near-perfect tuning when a weak plasma is introduced because small alterations in the propagation path change the strength of the horns standing wave, and this produces either a loss or even a gain in the transmitted signal. Before a test, the phase-amplitude bridge is nulled by adjusting the reference phase shift and attenuation until no signal is detected by the mixed signal detecting crystal. In order to test the tuning and the interaction between the two arms, carefully fitted polymer foam blocks having known dielectric and loss properties were placed between the windows in the nozzle. Measured phase shifts agreed with predicted values to within 10%. The shock tube supplying the tunnel was fitted with a closure plate which blanked off the nozzle entrance and was operated at conditions typical of those used for nozzle runs. Interferometric data were then obtained to determine the disturbance levels of recoil motion and of elastic wave propagation. It was found that these mechanical effects could be safely neglected in the interpretation of the data.

B.   Nonequilibrium Ionization Measurements

The shock tube supplying the tunnel was operated with hydrogen driver gas at pressures from 500 psi to 12,000 psi and over an incident shock Mach number range of 6.7 to 10.7. These conditions gave a range of reservoir states from $T_o = 3500°K$, $p_o = 25$ atm to $T_o = 7100°K$, $p_o = 650$ atm. The low pressures and Mach numbers were selected to minimize the air ionization at the test

station. Therefore the electron density levels which were measured (Fig. 17) serve as a measure of the maximum impurity ionization level. Ionization curves for sodium (I = 5.12 ev) show that for 10^{13} atoms/cc 70% of the atoms are ionized at 3500°K and that there is complete ionization at 4000°K. Consequently, at all higher temperatures there should be no increase in the number of impurity electrons.

Microwave records were obtained for reference arm power, plasma reflected power, plasma transmitted power, and mixed signal power. The signal level through the reference arm remained constant during all runs indicating no unwanted interaction of this signal with the plasma in the test arm. The power reflection coefficient of the plasma was less than 0.1% for all experiments. The data were reduced to phase-shift readings by adjusting the phase-shifter and attenuator in the reference arm to duplicate the combination of transmitted power level and mixed signal level recorded at each time during the experiment. Attenuation due to the plasma could be obtained because it was larger than the horn detuning effect described above. Some transmission loss may be accountable on the basis of near-field radiation pattern distortion due to slight transverse nonuniformity of the plasma. The magnitude of this gradient, which is perpendicular both to the flow and the microwave beam, has been calculated to give no more than 4% variation about the mean electron density. In the following subsection C on theoretical interpretation, both the origin and the method of prediction of this nonuniformity are discussed in greater detail. Measurement of attenuation is more sensitive to this type of distortion than measurement of phase shift because of the directionality of the horns. However, auxiliary detectors situated at many locations failed to detect any refracted signal during the runs.

AF-1500-A-1

Each phase-shift record obtained from the reduction procedure described above first exhibited a sharp rise signifying the arrival of the leading compression wave preceding the gas originating in the reservoir. The rise was followed by an irregular but high level of signal which dropped to a plateau having a comparatively low noise level when the (u-a) wave arrived signaling the end of the tunnel starting. This plateau signified the useful, quasi-steady test flow of air. After the first plateau the ionization dropped to a second plateau at a level about one-half that of the first. Finally, the level dropped back to zero. The end of the useful test flow is marked by the first measurable effect of driver gas dilution of the air terminating the first plateau. It seems plausible that the second plateau arises from the nonequilibrium ionization frozen in the quenched combustion zone originating from an air-hydrogen diffusion flame sustained by interfacial mixing.

C.   Interpretation of the Results

1.   Establishment of Useful Testing Times

The explanation of events in the ionization histories was qualitatively supported by theoretical estimates of the timing of the starting flow. The starting process in a shock tunnel operating behind the reflected shock wave is discussed in Ref. 42. That report shows that the tunnel will start rapidly when the initial pressure in the nozzle is very low. The ideal minimum time for steady flow to be established is then the time required for a nonsteady expansion fan which is initiated at the throat to sweep pass the testing station. Combining this computed time with the time required for the incident shock wave to travel from the triggering station to the end wall consistently predicted a starting time for steady flow which was approximately 100 μsec less than the measured value. This discrepancy is not surprising because the actual starting process is two-

dimensional with waves propagating from the walls through the boundary layer to the center of the flow as well as propagating axially along the nozzle. This difference in starting time became very noticeable when a correlation with heat transfer and stagnation pressure in the six foot test section was made. At this station the time difference was the order of several hundred microseconds.

Uncertainties due to interface mixing prevent a prediction of the end of useful test time.[42] However, the ionization records showed rather sudden changes to negative slopes at the end of the first plateau. The interface travels down the nozzle on a u-trajectory preceeded by a $(u + a)$ wave; however, because of the low temperatures, both the wave and interface arrive in the test section at nearly the same time. Extrapolation of the end of steady flow as measured by the microwave interferometer to the six foot test section again indicated a discrepancy with the heat transfer and stagnation pressure of several hundred microseconds.

While neither the correlation of the beginning or end of the useful test time in the test section can be made on the basis of a simple one-dimensional wave analysis, the agreement of the total time difference from beginning to end was in general fairly good. The actual testing times were much less than that predicted on the basis of an ideal interface. However, useful test flow was achieved over a wide range of conditions. The trend of the data indicates that testing time increases somewhat as the reservoir pressure level increases and that it decreases as the Mach number increases for Mach numbers between 6.7 and 10.7. Extrapolation of test section testing time versus incident shock strength to zero time gives an intercept at a Mach number in the vicinity of 11. These results indicate that the interface which terminates the steady-flow region arrives far earlier than ideal shock-tube theory predicts (based on planar interface).

2. Interface Mixing Phenomena

As pointed out in the preceding section the availability of the microwave interferometer technique has proved a reliable method of determining the arrival of the interface in the six-foot shock tunnel. Previously, reliance was placed on a combination of pitot static and heat transfer instrumentation to establish interface position. With high-enthalpy drivers this has not always proved reliable. With microwave instrumentation the observation of the departure of available testing time in the six-foot shock tunnel proved to be at variance with previous experience obtained in shock tunnels at Cornell Aeronautical Laboratory. Previously, utilizing cold helium as the driver in the 11" by 15" shock tunnel, better than 60% of the available test time could be achieved, and even with cold hydrogen at least 50% of the test time would be achieved.[7] In general, the pressures within the shock tube were very high during shock tunnel operation and this reduction in testing time was attributed to mixing initiated by rupturing of the diaphragm rather than to viscous phenomena.[43] The reduction of testing time in the present shock tunnel is a result of complex gasdynamic phenomena and may be directly related to the specific design of the six-foot shock tunnel. In the succeeding paragraphs, an explanation is offered; however, until definitive experiments are carried out this should be regarded as tentative.

As indicated in the description of the shock tunnel facility, heated hydrogen is utilized to obtain tailoring for high-enthalpy operation. The performance indicated that ideal shock-tube theory must be modified when utilizing heated drivers. In this shock tube, the driver is heated externally prior to a run in order to avoid the development of internal thermal stresses. In order to prevent damage to the O-rings sealing the diaphragm, cooling coils are placed adjacent to the diaphragm region. This leads to a temperature gradient within the driver so that prior to each run, cold hydrogen

AF-1500-A-1

is collected in the vicinity of the diaphragm. Immediately after bursting of the diaphragm, only cold hydrogen is available as the driver gas. Subsequently, as the cold hydrogen is used up, it must in turn be accelerated by the heated hydrogen. This difficulty is further enhanced by the large degree of chambrage (area contraction) incorporated into the shock tube design with the hope of increasing performance. The area contraction lowers the velocity within the driver, and a longer time is required before the cold hydrogen is swept out of the driver. Thus, the driven gas is effectively accelerated by a driver gas with an axial temperature gradient.

This type driver introduces new and unanticipated problems in relationship to tailoring. Tailoring requires that the driver-driven interface be so matched that the reflection of the shock wave from the nozzle end does not create further reflections. In the case of a driver of uniform temperature, the tailoring conditions can be directly calculated. However, with the temperature gradient in the driver, no formal tailoring condition can be found. The interface between the air and the hydrogen generally involves a density gradient which is expected to be unfavorable from the viewpoint of Taylor stability,[44] and this condition is further complicated by the observation of combustion at the interface. Tailoring, utilizing the heated hydrogen driver, is not normally calculated but is based on observation of the pressure history in the shock tube and the examination of the available testing time. Also, equilibrium interface operation[7,45] is often used. This technique employs secondary reflections from the interface to further increase the enthalpy, and this operating condition tends to produce regions which promote Taylor instability. Careful monitoring of the flow then becomes mandatory.

In view of the complexity of the phenomena associated with the reduction of testing time during current operations of this shock tunnel, it would be

unwise at the present time to generalize about the factors involved in this testing time loss. Currently a research program is underway to study the aspects of tailored instability as they affect interface mixing, as well as a program of modification to the shock tunnel in order to extend its range of operation.

3. Deionization Rate Constant Experiment

As demonstrated previously,[19,33] the electron density at a given area ratio in nonequilibrium expanding airflows is relatively insensitive to reservoir pressure, but is almost inversely proportional to the rate constant. Estimates of the electron density were made with the aid of numerical solutions of nonequilibrium nozzle flows from reservoir temperatures from 5000°K to 8250°K at a few typical reservoir pressures. The calculations were performed using the program described in Ref. 32 and the neutral particle kinetic data shown in Table 1. Reaction 10 (forward and reverse) shown in Table 2 was the only ionization reaction considered for the reasons given at the beginning of this section. A polynomial curve fit of the geometrical area function of the primary nozzle contour was employed. Boundary-layer corrections based on the methods of Ref. 41 were applied to get the gasdynamic conditions at the exit of the nozzle; however, the electron mass concentration at the geometrical exit area was used. This is a better approximation than the effective area ratio because the slope of the area function is small near the exit. Hence, the integrated residence time would be more nearly described by choosing the nonequilibrium ionization level based on actual axial distance rather than effective area ratio.

Since the chemistry of the neutral particles was essentially frozen at the conditions of the experiment, ideal gas calculations were employed for obtaining conditions after the expansion fan which turns the flow through 10°.

Frozen vibration was assumed to obtain the effective specific heat ratio. Ionization relaxation was calculated for the inner and outer streamlines entering the microwave beam. Line segment approximations with average densities were used for the outer streamline. Computation of ionization relaxation for the inner streamline was straightforward since the residence time in the expansion fan is approaching zero. Over-all reductions in electron mass concentrations between primary nozzle exit and the microwave beam were in the near vicinity of 30% for all cases. Greater recombination along the outer streamline than the inner streamline resulted in a plasma gradient which was mutually perpendicular to the flow velocity and the microwave propagation direction. As mentioned previously, this variation never resulted in nonuniformity exceeding 4% about the mean value. The extent of recombination in the expansion fan was rather insensitive to the computational model; therefore, no higher approximations for the outer streamline were sought.

Figures 17 and 18 show the preliminary data obtained from the experiments. The error bars are based only on the uncertainty in reading the oscilloscope traces. They do not include effects of detuning, errors in the calibration procedure, assumption of a one dimensional microwave beam for data reduction, or neglect of electron density gradients in the boundary layer. The electron density was found to be independent of the pressure level. This insensitivity was also exhibited by the results from the complete nonequilibrium flow solutions.

The atom and molecule cross-sections used for predicting the electron collision frequencies in Fig. 18 were taken from Fig. 7 in Ref. 46. The measured electron collision frequencies tend to be higher than those predicted. This difference was most pronounced for the runs where the pressure varied between 75 and 100 atmospheres. Assuming that the average temperature of

the electrons corresponds to the local gas temperature the collision frequency would be 4×10^8 cps, however, if the electron temperature was at the temperature the gas had at the nozzle throat (an approximation to the gas vibrational temperature at the testing station) the collision frequency would have been 1.3×10^9 cps. The measured value of 3×10^9 cps fell outside of this range. Corrections to the collision frequency which account for electron-ion collisions, 2×10^7 cps, electron-sodium atom collisions, 10^4 cps (assuming 10^{13} atoms/cc in the reservoir), and electron-copper atom collisions, 10^7 cps (assuming 0.1 cc of nozzle throat is vaporized, an extreme upper limit) are incapable of accounting for the differences. The effect of an electron density gradients in the boundary layer would be to decrease both the phase change and the attenuation of the transmitted signal.[47] Therefore the measured electron collision frequency in Fig. 18 would be decreased and the electron densities in Fig. 17 would, in general, be increased if this effect were taken into account. The quantitative effect of this gradient on the reduced data is at present not known. The main difficulty in correcting the data is in determining the distribution of electrons in the boundary layer. The more direct method would be to employ boundary layer bleeds just upstream of the measuring station and thus to avoid making this an important correction to the data.

The value of the dissociative-recombination rate constant which gives good agreement with the measured electron densities is of the same order of magnitude as that in Ref. 18. A more precise determination of this rate constant will be made following additional experiments which are now underway. Specifically, runs with nitrogen instead of air as the test gas are being made to verify that the measured phase shift and attenuations are not due to impurities. Furthermore a simultaneous reading S-band interferometer placed near the

AF-1500-A-1

entrance of the Fiberglas portion of the conical nozzle should yield further information on the temperature dependence of the rate constant. Extension of the theoretical studies may shed additional light on the questions of unimolecular processes posed in Ref. 21 because of the higher density levels in the present experiment. Values of the specific rate constant will be reported after further studies are made.

In summary, the microwave diagnostic methods commonly used in gaseous discharge physics have proved to be useful tools in studying not only nonequilibrium ionization in shock tunnel flows, but also the basic gasdynamic processes, occuring in such flows. Considering the state of knowledge in high-temperature chemical kinetics, the rate information indicated by the preliminary data does not disagree seriously with that reported elsewhere.[20,21,48]

AF-1500-A-1

V. SUMMARIZING REMARKS

Shock tunnel methods have been discussed in the context of ionized flow studies. Certain features of the six-foot facility at the Cornell Aeronautical Laboratory have been described. The large test section and the Fiberglas nozzle render it useful in the investigation of plasma flows appropriate to hypersonic flight.

One of the most significant considerations in such shock tunnel research is that of nonequilibrium phenomena both in the tunnel flow and in the flow near a body. Emphasis in the present work has been on ionization mechanisms in these nonequilibrium flows. For certain purposes of electromagnetic studies, rather complex mechanisms may be necessary for blunt-body flows of present day engineering interest occurring under ballistic re-entry conditions. Super-orbital flight poses re-entry problems involving large amounts of energy invested in ionization and requiring the use of generalized ion-kinetics for realistic determination of flow-field gasdynamics. At pressures and temperatures encountered in nozzle flows in existing shock tunnel facilities, the comparatively simple ionization models presently in use seem to suffice for large expansions.

Microwave interferometric measurements of electron density have been described. The records indicate that the effects of the driver gas terminate the useful test flow earlier than would be predicted on the basis of simple shock tube theory. The simplicity of ion kinetics in the shock tunnel flow permits the study of a single deionization process. Preliminary data agree reasonably well with previously reported values of the dissociative recombination rate constant for nitric oxide ions and electrons, however the quantitative effects of impurities in this facility have not yet been fully determined.

AF-1500-A-1

REFERENCES

1. Glick, H. S., Interaction of Electromagnetic Waves with the Plasmas of Hypersonic Flows. ARS Preprint 2174-61 of a paper delivered at the Space Flight Report to the Nation, October 1961.

2. Hines, C. A. and Simons, R. A., An Experimental Study of Electromagnetic Wave Propagation Through an Ion Sheath, Part I. Instrumentation of Hypersonic Shock Tunnel for Propagation Measurements. WADD TR 60-276, July 1960.

3. Huber, P. W. and Gooderum, P. B., Experiments with Plasmas Produced by Potassium-Seeded Cyanogen-Oxygen Flames for Study of Radio Transmission at Simulated Re-entry Vehicle Plasma Conditions. NASA TN D-6270, January 1961.

4. Charters, A. C., The Free Flight Range: A Tool for Research in the Physics of High-Speed Flight. ARS Preprint 1984-61 of a paper presented at the International Hypersonics Conference, August 1961.

5. Siperly, B. H., Bradford, W. R. and Short, W. W., Microwave Study of Wakes Behind Hypervelocity Projectiles (U). AMRAC Proceedings, Vol. V, Part I (SECRET), November 1961.

6. Gibson, W. E. and Marrone, P. V., A Similitude for Nonequilibrium Phenomena in Hypersonic Flight. Paper presented at AGARD Conference on "High Temperature Aspects of Hypersonic Flow," 3-6 April 1962.

7. Hertzberg, A., Wittliff, C. E., and Hall, J. G., Summary of Shock Tunnel Development and Application to Hypersonic Research. Cornell Aero. Lab. Rept. No. AD-1052-A-12, AFOSR TR 60-139, July 1961; also, Hypersonic Flow Research, Edited by F. R. Riddell, Academic Press, New York (1962).

8. Wittliff, C.E., Wilson, M.R., and Hertzberg, A., The Tailored-Interface Hypersonic Shock Tunnel. J. Aero. Sci., Vol. 26, No. 4, April 1959.

9. Gibson, W.E., Dissociation Scaling for Nonequilibrium Blunt-Nose Flows. ARS Journal, Vol. 32, No. 2, February 1962.

10. Hall, J.G., Eschenroeder, A. Q., and Marrone, P. V., Inviscid Hypersonic Air Flows with Coupled Nonequilibrium Processes. IAS Paper No. 62-67 presented at the 30th Annual Meeting, January 22-24, 1962.

11. Hilton, J., Fabian, G.J., Golian, T.C., Wilson, M., and Somers, L., Development and Performance of the CAL Six-Foot Shock Tunnel. Presented at the Second National Symposium on Hypervelocity Techniques, Denver, Colo., March 20-21, 1962.

12. Wittliff, C. E. and Wilson, M.R., Nozzle Flow Study and Flow Angularity Measurements in the Hypersonic Shock Tunnel. Cornell Aero. Lab. Rept. No. AD-917-A-3, Part II, WADC TR 58-401, December 1958.

13. Vidal, R.J., Transient Surface Temperature Measurements. Cornell Aero. Lab. Rept. No. 114, March 1962.

14. Skinner, G.T., Analog Network to Convert Surface Temperature to Heat Flux. ARS Journal, Vol. 30, No. 6, pp. 569-570, June 1960.

15. Skinner, G.T., Calibration of Thin-Film Gauge Backing Materials. ARS Journal, Vol. 31, No. 5, pp. 671-672, May 1961.

16. Marrone, P.V. and Hartunian, R. A., The Performance of Thin-Film Thermometers in Partially Ionized Shock-Tube Flows. Phys. Fluids, Vol. 2, No. 2, p. 719, November/December 1959.

17. Glick, H.S., Theory of the Thin-Film Bolometer. Submitted for publication in The Review of Scientific Instruments.

18. Hammerling, P., Teare, J. D., and Kivel, B., Nonequilibrium Electrical and Radiative Properties of High-Temperature Air, Nitrogen, and Oxygen. Proceedings of the 4th International Conference on Ionization Phenomena in Gases, North-Holland Publishing Co., pp. 1092-1097, Amsterdam 1960.

19. Eschenroeder, A. Q., Ionization Nonequilibrium in Expanding Flows. ARS Journal, Vol. 32, No. 2, pp. 196-203, February 1962.

20. Lin, S. C., Neal, R. A., Fyfe, W. I., Rate of Ionization Behind Shock Waves in Air, Experimental Results. AVCO-Everett RR 105, AFBMD TR-60-216, September 1960.

21. Daiber, J. W. and Glick, H. S., Plasma Studies in a Shock Tube. Proceedings of Symposium on the Dynamics of Gaseous Plasmas. To be published.

22. Squires, B. E., Jr., Cross-Section for Dissociative Recombination of Nitric Oxide. Penn. State Univ., Ionospheric Research Laboratory Scientific Report 144, AFCRL 242, January 1, 1961.

23. Eyring, H., Hirshfelder, J. O., and Taylor, H. S., Free Radical Combination Reactions. J. Chem. Phys., Vol. 4, p. 479, 1936.

24. Kennard, E. H., Kinetic Theory of Gases. McGraw-Hill Publishing Co., New York, p. 441, 1938.

25. Ree, T. S., Ree, T., Eyring, H., and Fueno, T., Activated Complexes of Fast Bimolecular Reactions. J. Chem. Phys., Vol. 36, No. 1, pp. 281-286, January 1962.

26. Beran, M. J., A Note on Nonequilibrium Species Concentrations in Air. J. Atmos. & Terres. Phys., Vol. 21, No. 4, pp. 293-295, July 1961.

AF-1500-A-1

27. Meyerott, R. E. and Landshoff, R. M., Physics of the Ionization Processes in Air. Lockheed Missile Systems Division Report LMSD 48361, December 1958.

28. Krasovskii, V. I., The Effective Recombination Coefficient in the Ionosphere. Akademiya Nauk SSSR, Izvestiya Seriya Geofizicheskaya, No. 4, pp. 103-110, 1957.

29. Nawrocki, P. J., Reaction Rates. Geophysics Corp. of America, Rept. 61-2-A, January 1961.

30. Massey, H. S. W., Recombination of Gaseous Ions. Advances in Phys., Vol. 1, p. 395, 1952.

31. Mitra, S. K., The Upper Atmosphere. Asiatic Society, 1952; also Science and Culture, Vol. 9, p. 46, 1943.

32. Eschenroeder, A. Q., Boyer, D. W., and Hall, J. G., Nonequilibrium Expansions of Air with Coupled Chemical Reactions. Cornell Aero. Lab. Rept. No. AF-1413-A-1, AFOSR 622, May 1961; extended form to be published in Phys. of Fluids, Vol. 5, No. 5, May 1962.

33. Eschenroeder, A. Q. and Daiber, J. W., Nonequilibrium Ionization in Shock Tunnel Flows. ARS Journal, Vol. 31, No. 1, p. 94, January 1961.

34. Wurster, W. H. and Marrone, P. V., Study of Infrared Emission in Heated Air. Cornell Aero. Lab. Repts. QM-1373-A-1 through A-4, July 1959 through June 1961.

35. Marrone, P. V. and Eschenroeder, A. Q., Nonequilibrium Airflow About the Nose of a Blunt Hypersonic Body. Paper E10, Am. Phys. Soc. Div. of Fluid Dynamics, November 1961.

36. Massey, H. S. W. and Burhop, E. H. S., Electronic and Ionic Impact Phenomena. Oxford Univ. Press, London, 1952.

37. Bauer, S.H. and Tsang, S.C., Mechanisms for Vibrational Relaxation at High Temperatures. To be published in the J. Chem. Phys.

38. Treanor, C.E. and Marrone, P.V., The Effect of Dissociation on the Rate of Vibrational Relaxation. Cornell Aero. Lab. Rept. No. QM-1626-A-4, February 1962.

39. Goldstein, L., Electrical Discharges in Gases. Advances in Electronics, Vol. 7, p. 399, 1955.

40. Wharton, C.C., Microwave Diagnostics for Controlled Fusion Research. Plasma Physics, Chap. 12, J.E. Drummond, Ed., McGraw-Hill Publishing Co., New York, 1961.

41. Burke, A.F. and Bird, K.D., The Use of Conical and Contoured Expansion Nozzles in Hypervelocity Facilities. Cornell Aero. Lab. Rept. No. 112, January 1962 (based on a paper presented at the Second National Symposium on Hypervelocity Techniques, Denver, Colo., March 19-20, 1962).

42. Glick, H.S., Hertzberg, A., and Smith, W.E., Flow Phenomena in Starting a Hypersonic Shock Tunnel. Cornell Aero. Lab. Rept. No. AD-789-A-3, AEDC-TN-55-16, March 1955.

43. Roshko, A., On Flow Duration in Low-Pressure Shock Tubes. Phys. of Fluids, Vol. 3, p. 835, 1960.

44. Taylor, G., The Instability of Liquid Surfaces When Accelerated in a Direction Perpendicular to Their Planes, I., Proc. Roy. Soc., Vol. A201, p. 192, 1950.

45. Holder, D.W. and Schultz, D.L., The Duration and Properties of the Flow in a Hypersonic Shock Tunnel. Hypersonic Flow Research, Ed. by F. R. Riddell, Academic Press, New York 1962.

46. Shkarofsky, I. P., Bachynski, M. P., and Johnston, S. W., Collision Frequency Associated With High Temperature Air and Scattering Cross-Sections of the Constituents. Electromagnetic Effects of Re-entry, Pergamon Press, 1961.

47. Albini, F. A. and Jahn, R. G., Reflection and Transmission of Electromagnetic Waves at Electron Density Gradients. Jour. Appl. Phys., Vol. 32, p. 75, 1961.

48. Gunton, R. C. and Inn, E. C. Y., Rates of Electron Removal by Recombination Attachment and Ambipolar Diffusion in Nitric Oxide Plasma. J. Chem. Phys., Vol. 35, No. 5, p. 1896, November 1961.

TABLE I

KINETIC DATA FOR REACTIONS OF NEUTRAL SPECIES
(SOURCES DISCUSSED AND CITED IN REFERENCES 10 AND 32)

$$k_{Fi} = A_i T^{n_i} \exp(-\theta_i/T) \, \text{cm}^3 \, \text{mole}^{-1} \, \text{sec}^{-1} \text{ FOR T in } °K$$

| i | REACTION | COLLISION PARTNER, M | | A_i | n_i | θ_i |
		DECELERATING FLOW SOLUTIONS	ACCELERATING FLOW SOLUTIONS			
1	$O_2 + M \overset{k_{F_i}}{\underset{k_{B_i}}{\rightleftharpoons}} 2O + M$	O_2	O_2	3.6×10^{21}	-1.5	59380
2		O	O	2.1×10^{18}	-0.5	59390
3		N_2, N, NO	N_2	1.2×10^{21}	-1.5	59380
4	$N_2 + M \rightleftharpoons 2N + M$	N_2	N_2	3.0×10^{21}	-1.5	113260
5		N	N	1.5×10^{22}	-1.5	113260
6		O_2, O, NO	O_2, O, NO	9.9×10^{20}	-1.5	113260
7	$NO + M \rightleftharpoons N + O + M$	N_2, O_2, O N, NO, Ar	N_2, O_2, O N, NO, Ar	5.2×10^{21}	-1.5	75490
8	$N + O_2 \rightleftharpoons NO + O$			1.0×10^{12}	0.5	3120
9	$O + N_2 \rightleftharpoons NO + N$			5.0×10^{13}	0	38000

49

AF-1500-A-1

TABLE II
KINETIC DATA FOR REACTIONS OF CHARGED SPECIES

$$k_{Fi} = A_i T^{n_i} \begin{cases} \text{cm}^3\ \text{mole}^{-1}\ \text{sec}^{-1} & \text{FOR } i = 10\text{-}12,\ 23\text{-}38 \\ \text{cm}^6\ \text{mole}^{-2}\ \text{sec}^{-1} & \text{FOR } i = 13\text{-}22,\ 39\text{-}49 \end{cases} \quad \text{AND } T \text{ in } {}^\circ K$$

i	REACTION	A_i	n_i	SOURCE
10	$e^- + NO^+ \xrightleftharpoons{\;k_{F10}\;} N + O$	1.8×10^{21}	-1.5	18
11	$e^- + O_2^+ \rightleftharpoons 2O$	1.9×10^{21}	"	"
12	$e^- + N_2^+ \rightleftharpoons 2N$	9.6×10^{21}	"	"
13	$N + e^- + O^+ \rightleftharpoons O + N$	6.0×10^{24}	-2.5	36
14	$O + e^- + O^+ \rightleftharpoons 2O$	6.0×10^{24}	"	"
15	$N_2 + e^- + O^+ \rightleftharpoons O + N_2$	2.0×10^{26}	"	"
16	$O_2 + e^- + O^+ \rightleftharpoons O + O_2$	9.0×10^{26}	"	"
17	$NO + e^- + O^+ \rightleftharpoons O + NO$	1.0×10^{28}	"	"
18	$N + e^- + N^+ \rightleftharpoons 2N$	6.0×10^{24}	"	"
19	$O + e^- + N^+ \rightleftharpoons N + O$	6.0×10^{24}	"	"
20	$N_2 + e^- + N^+ \rightleftharpoons N + N_2$	2.0×10^{26}	"	"
21	$O_2 + e^- + N^+ \rightleftharpoons N + O_2$	9.0×10^{26}	"	"
22	$NO + e^- + N^+ \rightleftharpoons N + NO$	1.0×10^{28}	"	"
23	$O + N_2^+ \rightleftharpoons N_2 + O^+$	7.8×10^{11}	0.5	18
24	$N_2 + O^+ \rightleftharpoons N + NO^+$	"	"	"
25	$O_2 + O^+ \rightleftharpoons O + O_2^+$	"	"	"
26	$NO + O^+ \rightleftharpoons O + NO^+$	"	"	"
27	$NO + O^+ \rightleftharpoons N + O_2^+$	"	"	"
28	$N + N_2^+ \rightleftharpoons N_2 + N^+$	"	"	"
29	$O_2 + N^+ \rightleftharpoons N + O_2^+$	"	"	"
30	$O_2 + N^+ \rightleftharpoons O + NO^+$	7.8×10^{11}	0.5	18
31	$NO + N^+ \rightleftharpoons N + NO^+$	"	"	"
32	$NO + N^+ \rightleftharpoons O + N_2^+$	"	"	"
33	$N^+ + O \rightleftharpoons N + O^+$	"	"	"
34	$O^- + N^+ \rightleftharpoons O + N$	1.0×10^{17}	-0.5	29
35	$O^- + O^+ \rightleftharpoons 2O$	1.0×10^{17}	"	30
36	$O^- + NO^+ \rightleftharpoons NO + O$	1.0×10^{18}	"	29
37	$O^- + O_2^+ \rightleftharpoons O_2 + O$	"	"	31
38	$O^- + N_2^+ \rightleftharpoons N_2 + O$	"	"	31
39	$M + O + e^- \rightleftharpoons O^- + M$	1.1×10^{19}	-1.0	29
40	$N + e^- + O_2^+ \rightleftharpoons O_2 + N$	6.0×10^{24}	-2.5	36
41	$O + e^- + O_2^+ \rightleftharpoons O_2 + O$	6.0×10^{24}	"	"
42	$N_2 + e^- + O_2^+ \rightleftharpoons O_2 + N_2$	2.0×10^{26}	"	"
43	$O_2 + e^- + O_2^+ \rightleftharpoons 2O_2$	9.0×10^{26}	"	"
44	$NO + e^- + O_2^+ \rightleftharpoons O_2 + NO$	1.0×10^{28}	"	"
45	$N + e^- + N_2^+ \rightleftharpoons N_2 + N$	6.0×10^{24}	"	"
46	$O + e^- + N_2^+ \rightleftharpoons N_2 + O$	6.0×10^{24}	"	"
47	$N_2 + e^- + N_2^+ \rightleftharpoons 2N_2$	2.0×10^{26}	"	"
48	$O_2 + e^- + N_2^+ \rightleftharpoons N_2 + O_2$	9.0×10^{26}	"	"
49	$NO + e^- + N_2^+ \rightleftharpoons N_2 + NO$	1.0×10^{28}	"	"

"M ≡ ANY COLLISION PARTNER

SPECIES NUMBER KEY

1. N_2	4. O	7. e^-	10. O_2^+	13. O^-
2. O_2	5. NO	8. NO^+	11. N^+	
3. N	6. Ar	9. N_2^+	12. O^+	

TABLE III

CHARGE TRANSFER RATE CONSTANTS
COMPUTED FROM THEORY OF REFERENCE 23

REACTION i	REDUCED MASS μ amu	POLARIZABILITY $\alpha \times 10^{26}$ cm^3	RATE CONSTANT $k_{Fi} \times 10^{10}$ cm^3 PARTICLE^{-1} sec^{-1}
23	10.18	80	6.58
24	10.18	176	9.75
25	10.66	160	9.10
28	9.34	128	8.66
29	9.74	160	9.51
30	9.74	160	9.51
33	7.47	80	7.64

TABLE IV

RATIOS OF ACTUAL TO EQUILIBRIUM AIRFLOW VARIABLES FOR
COUPLED-REACTION EXPANSIONS GIVING EQUILIBRIUM MACH NUMBER 20
REF. 32
$\ell = 1$ cm

T_0	6000°K		8000°K	
P_0	100 atm	1000 atm	100 atm	1000 atm
P/P_{EQ}	0.425	0.875	0.159	0.544
T/T_{EQ}	0.359	0.855	0.121	0.497
ρ/ρ_{EQ}	1.095	1.014	1.110	1.045
u/u_{EQ}	0.913	0.987	0.901	0.957
M/M_{EQ}	1.455	1.06	2.30	1.305
$Re_x/Re_{x_{EQ}}$	2.79	1.17	8.25	2.01

AF-1500-A-1

TEST SECTION

PRIMARY NOZZLE AND
FLOW TURNING SECTION

FIBERGLAS CONICAL
NOZZLE

SHOCK TUBE

BY-PASS AIR DUCT

1549
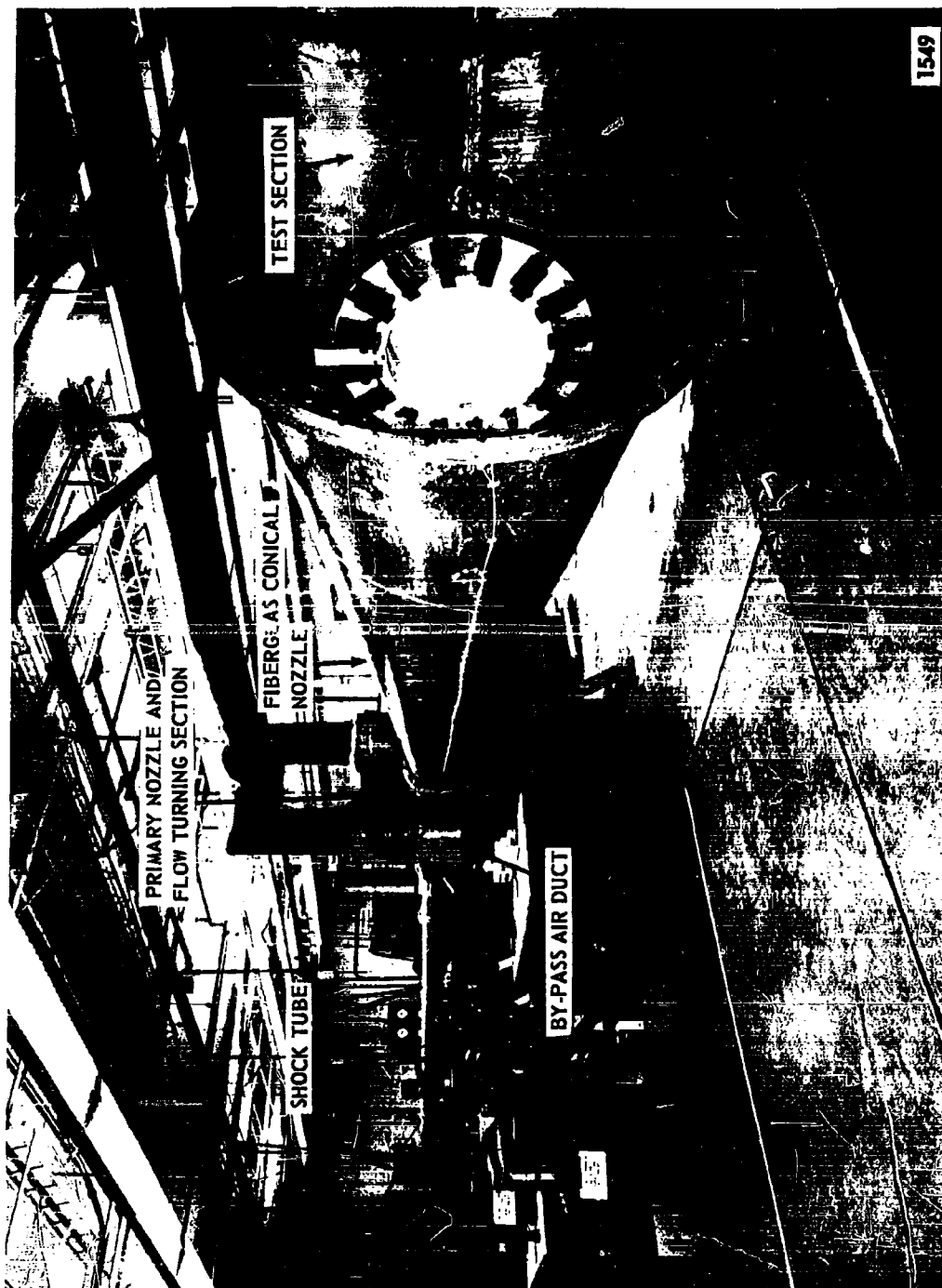
Figure 1 PHOTOGRAPH OF THE CAL 6-FT HYPERSONIC SHOCK TUNNEL

52

AF-1500-A-1

TERMINAL
NOZZLE

DUMP TANK

INTERCHANGEABLE
NOZZLE LIPS

10° FLOW DEFELECTION
PLATE

PRIMARY
NOZZLE

THROAT & SECONDARY
DIAPHRAGM

1548
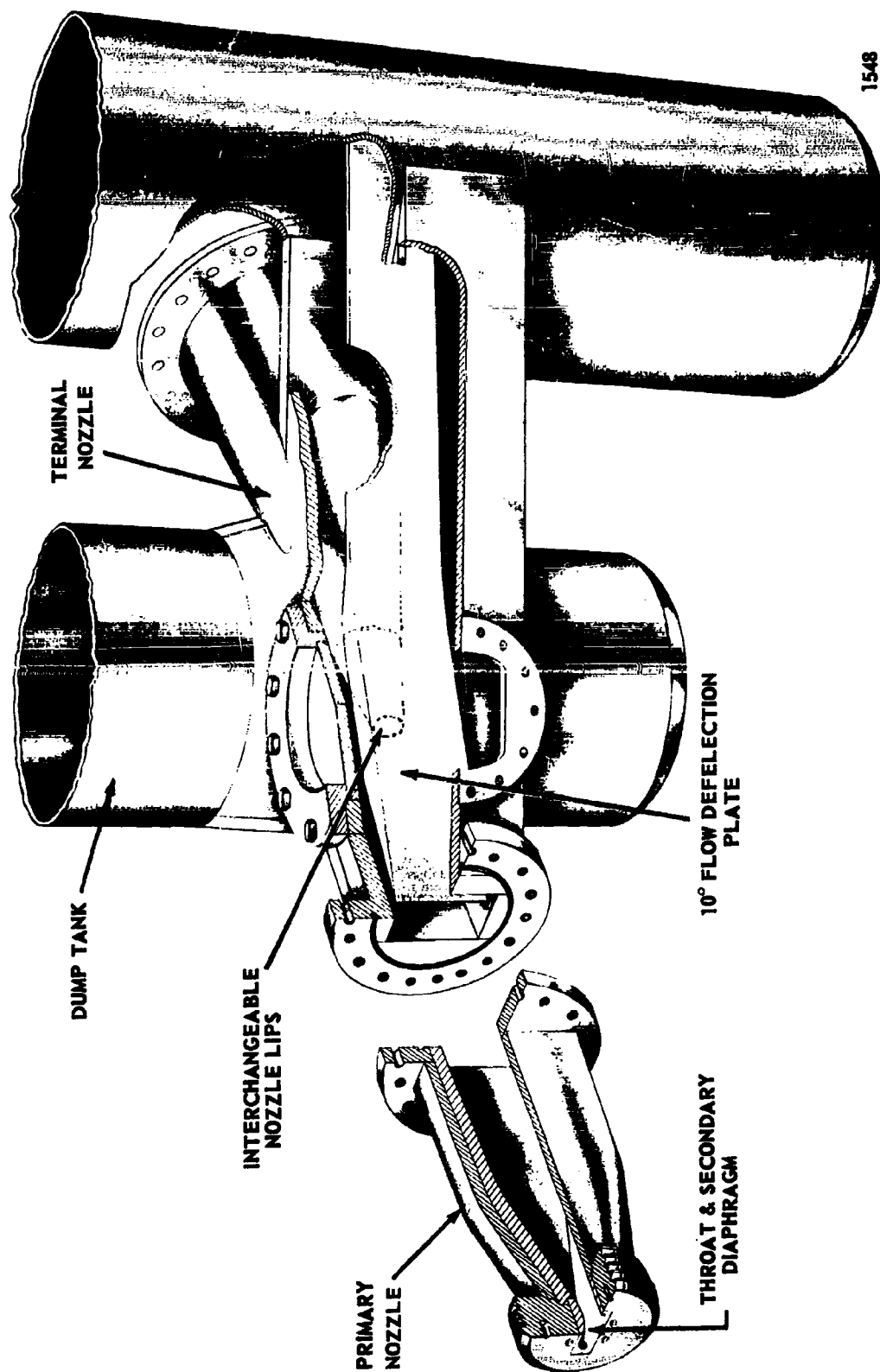
Figure 2 PRIMARY NOZZLE, FLOW-TURNING SECTION, AND CONICAL NOZZLE ENTRANCE FOR
THE CORNELL AERONAUTICAL LABORATORY 6 FT HYPERSONIC SHOCK TUNNEL.

AF-1500-A-1
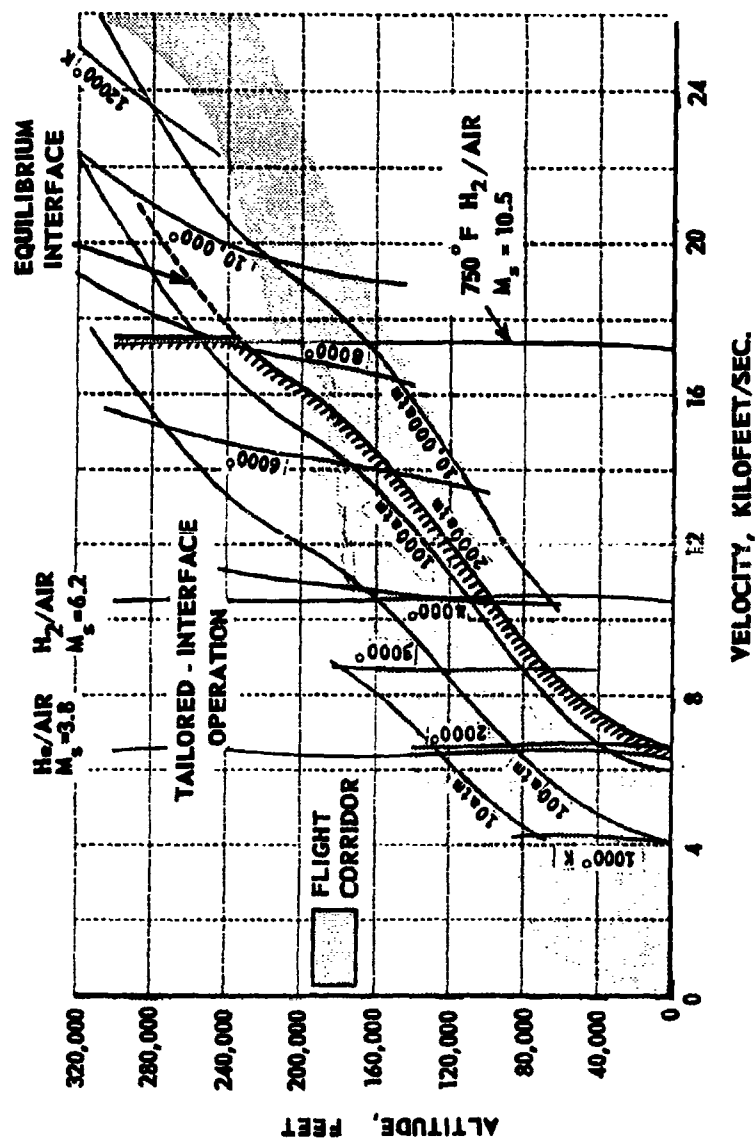
Figure 3 TUNNEL STAGNATION PRESSURES AND STAGNATION
TEMPERATURES REQUIRED FOR FLIGHT DUPLICATION

54

7.5

7.0
7500

6.5
$P_{T'} = 2700 \cdot 10{,}700$ psia
$T_{T'}$ (°K)

7000

$H_{T'}/RT_{T'}$

6.0
6000

5.5
5000

5.0
6   8   10   12   14

M_S

30   32   34   36   38

S/R
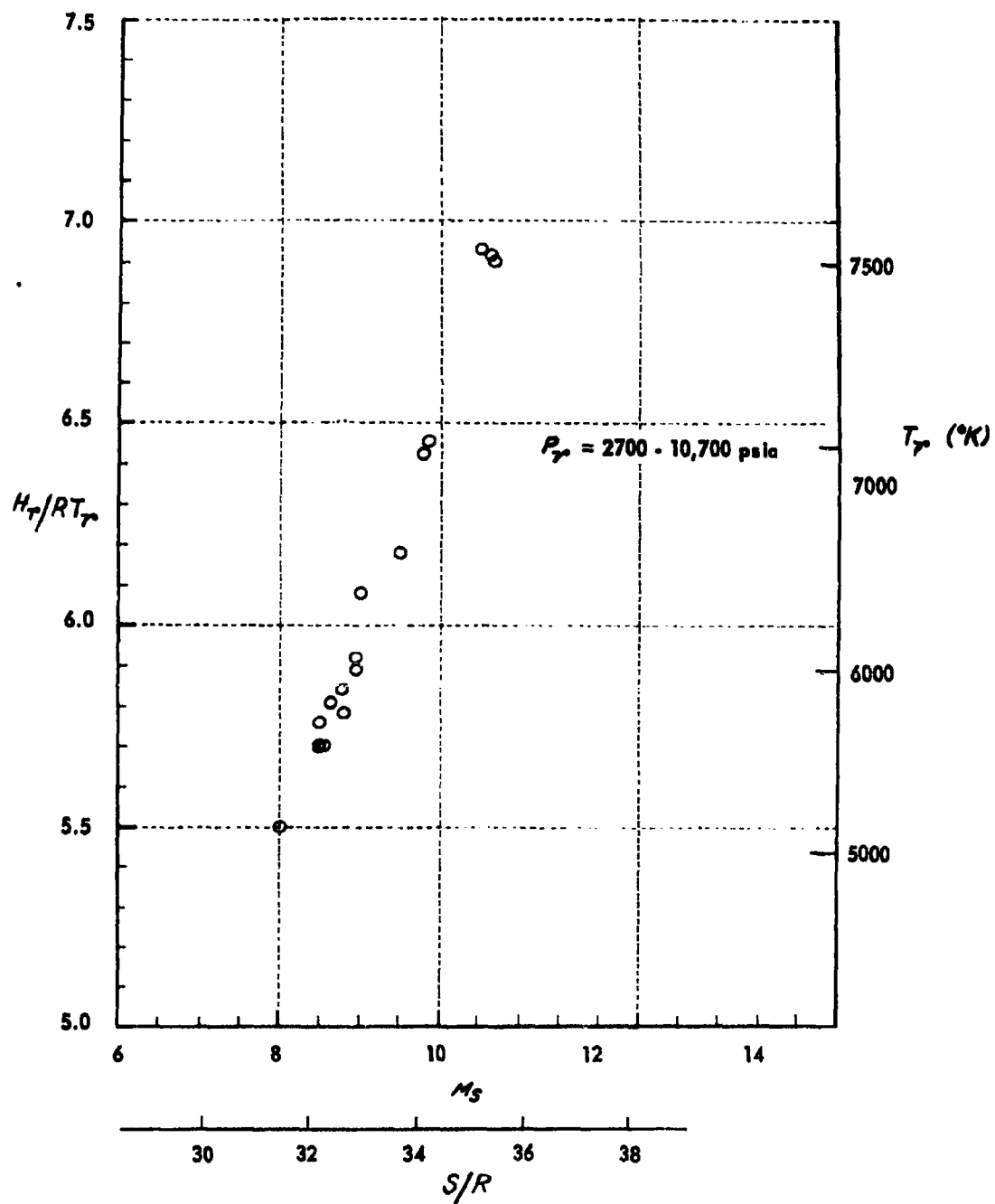
Figure 4   TAILORED AND EQUILIBRIUM INTERFACE OPERATION, 6' HYPERSONIC
SHOCK TUNNEL
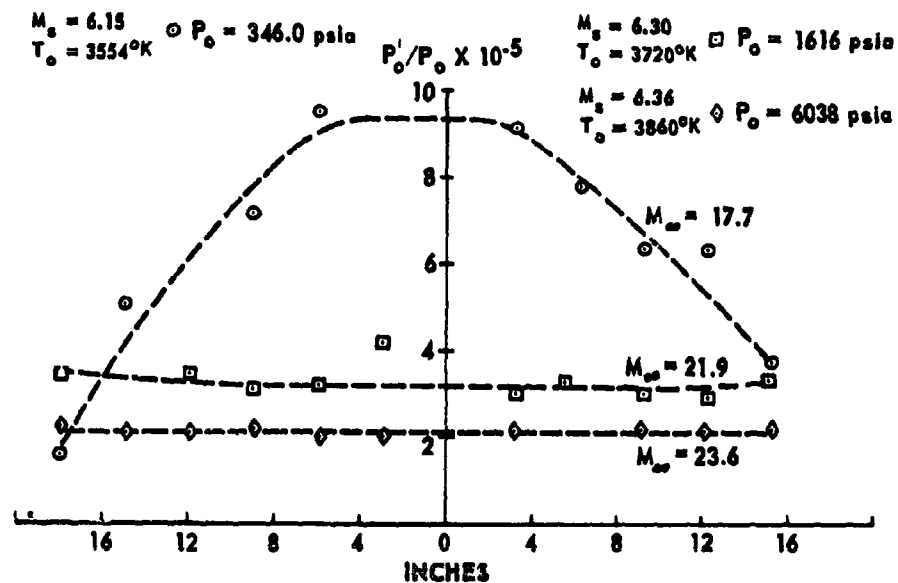
Figure 5 TEST SECTION PITOT PRESSURE DISTRIBUTION
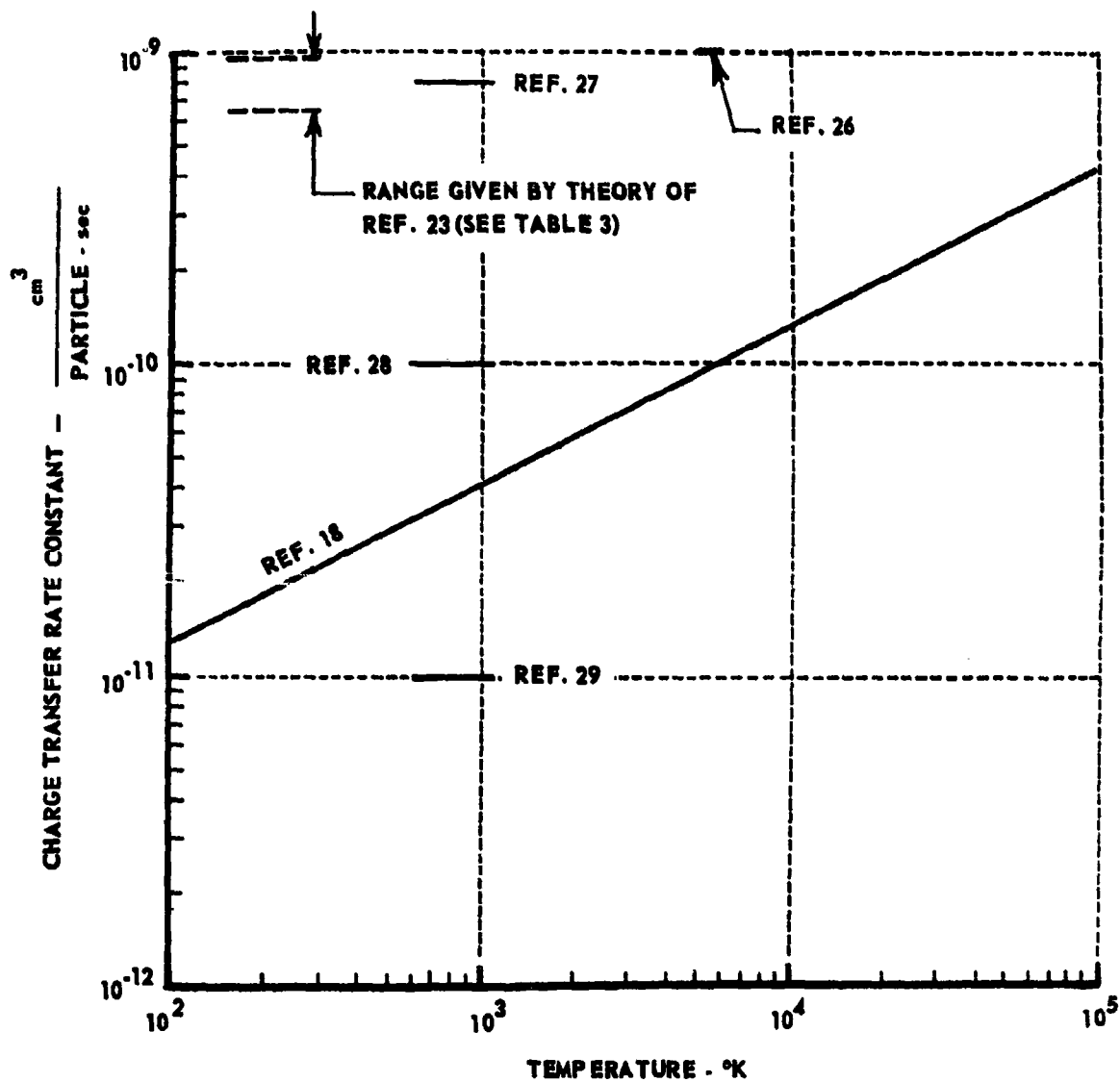
Figure 6 COMPARISON OF ESTIMATES FOR CHARGE TRANSFER
RATE CONSTANT
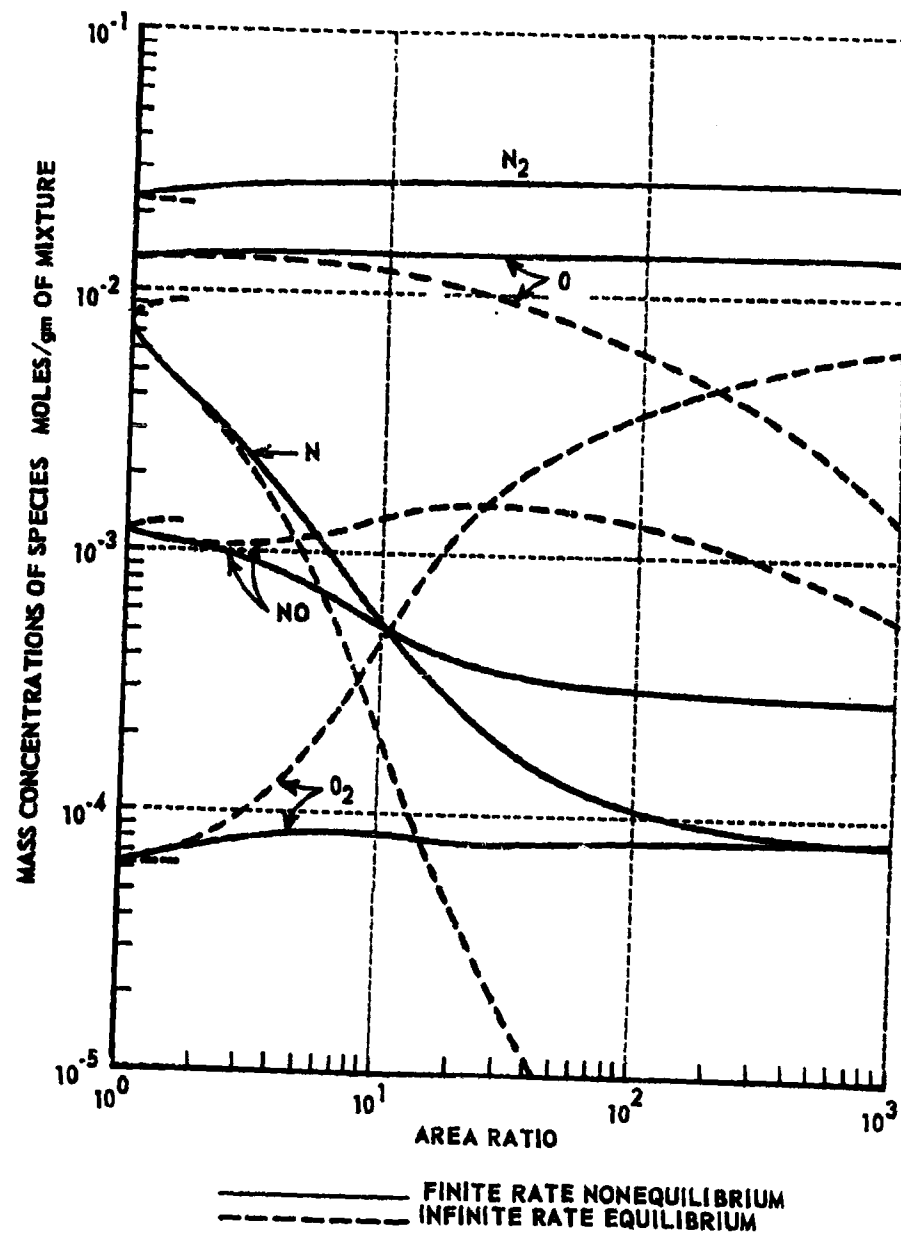
Figure 7 SPECIES DISTRIBUTIONS FOR AIR FLOW IN A HYPERSONIC NOZZLE
$T_0 = 8000°K,$ $P_0 = 100$ atm $\ell = 1$ cm

58   AF-1500-A-1
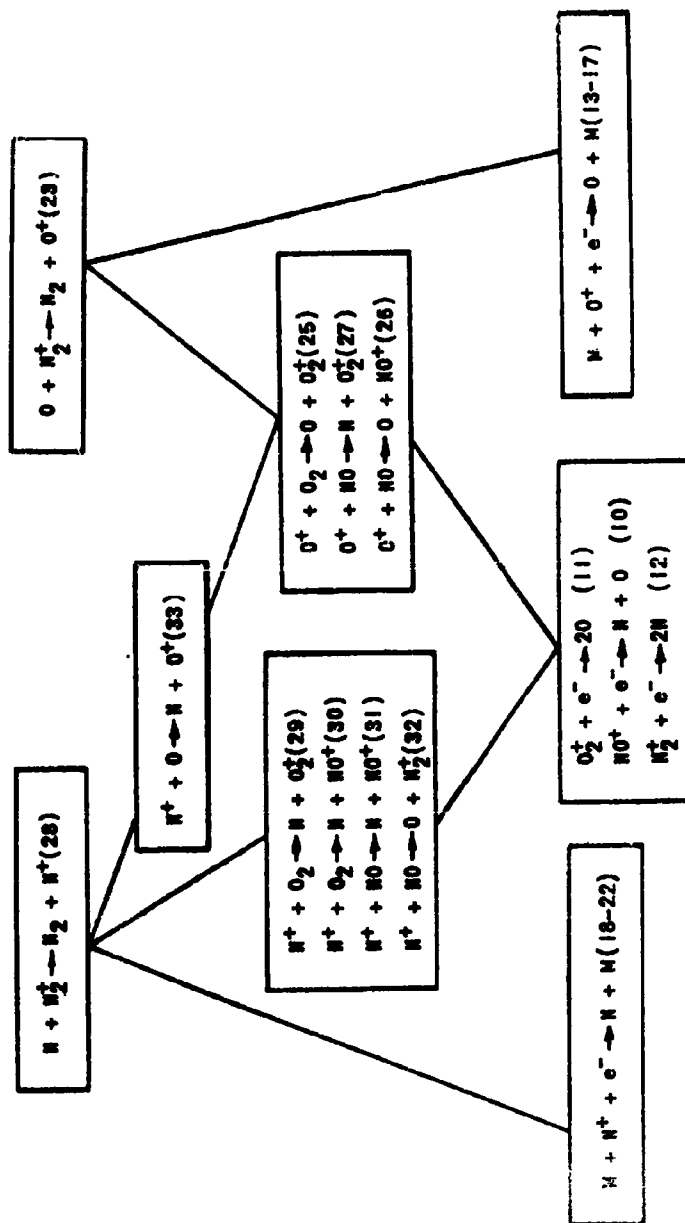
Figure 8 DEIONIZATION REACTION CHAINS FOR ELECTRONS AND SINGLY CHARGED POSITIVE-IONS IN AN AIR PLASMA

AF-1500-A-1
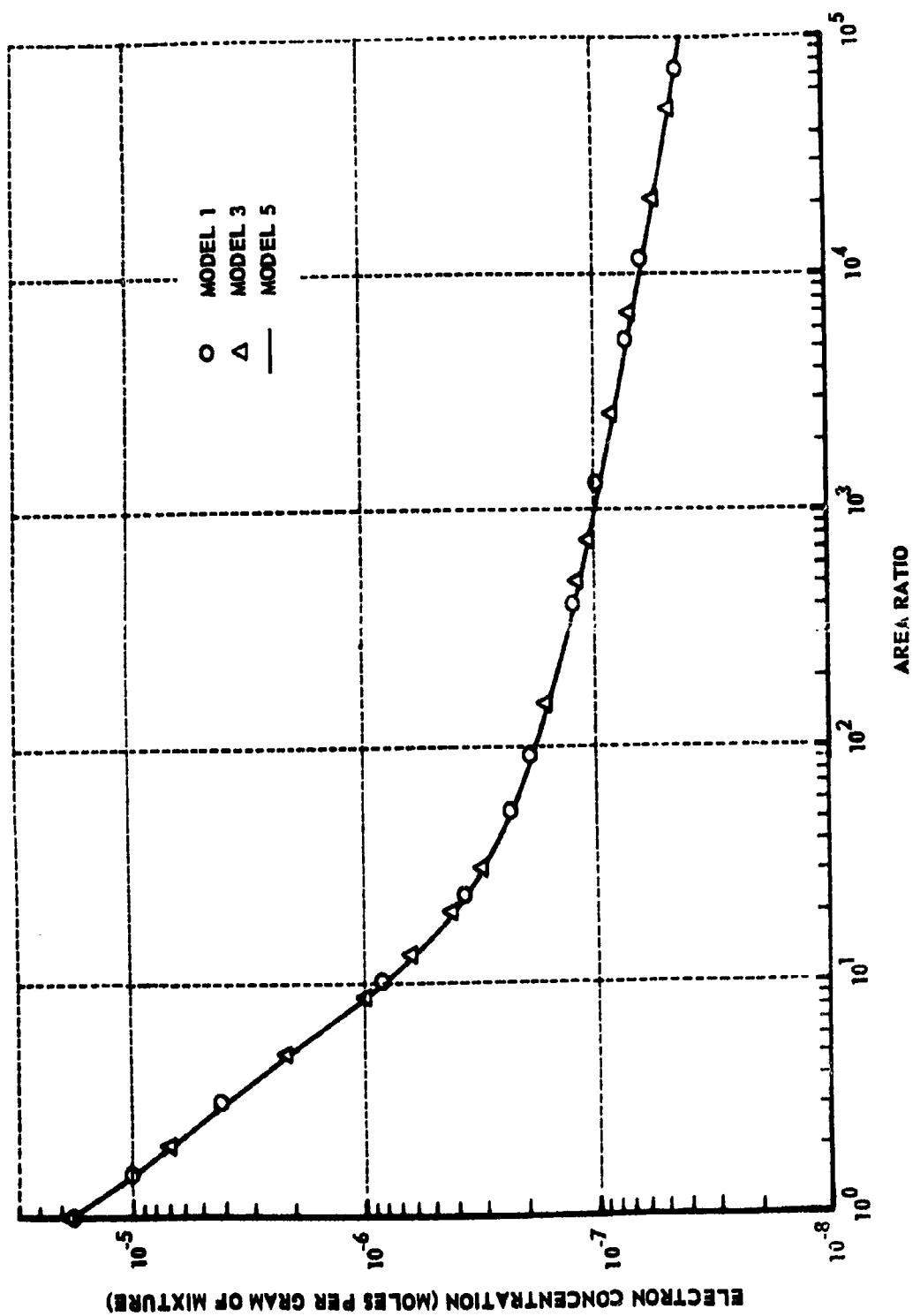
Figure 9 ELECTRON CONCENTRATION DISTRIBUTIONS FOR AIRFLOW IN A HYPERSONIC NOZZLE

$T_o = 8000°K;$ $P_o = 100$ atm; $\ell = 1$ cm
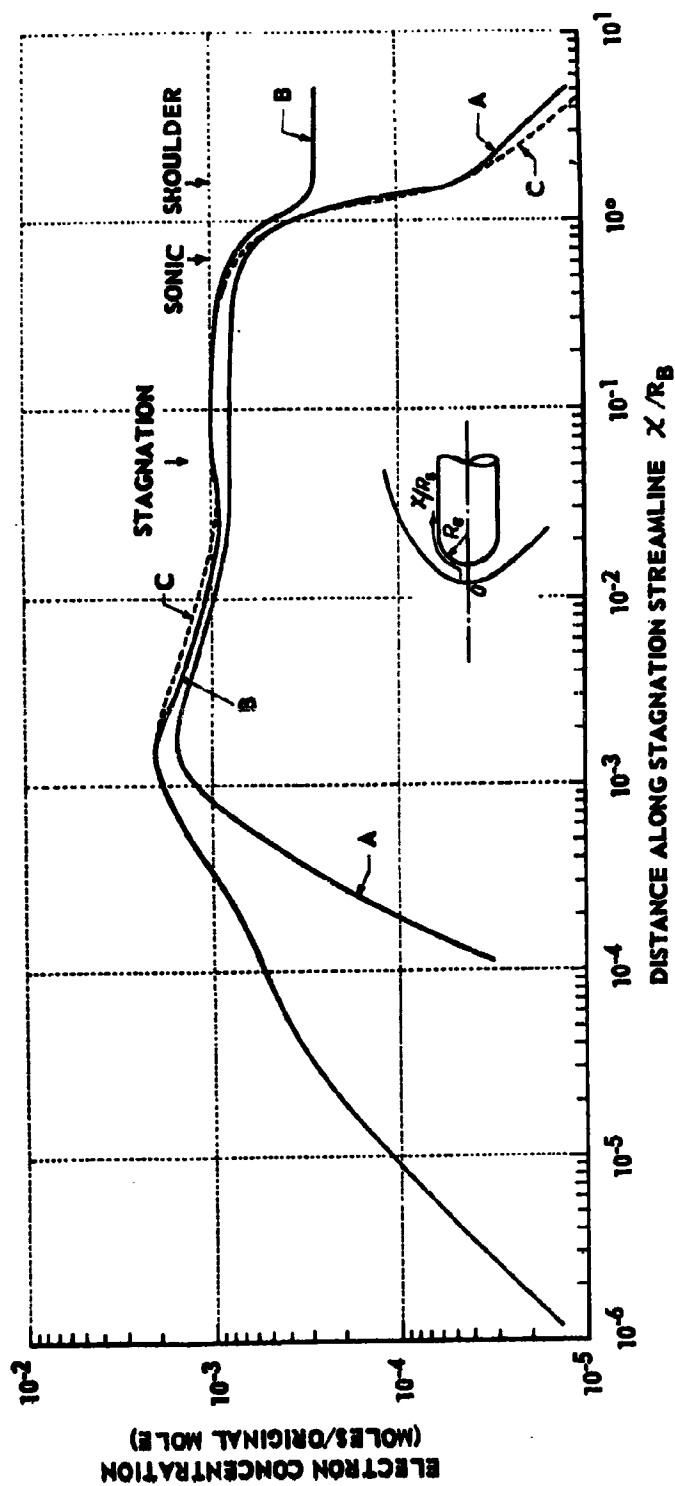
Figure 10 IONIZATION PROFILES ALONG A STREAM SURFACE ABOUT A HEMISPHERE-CYLINDER
VEL. = 23 kft/sec; ALT. = 150 kft; R_B = 1 ft (A,B & C REFER TO CASES DEFINED IN THE TEXT)

61   AF-1500-A-1
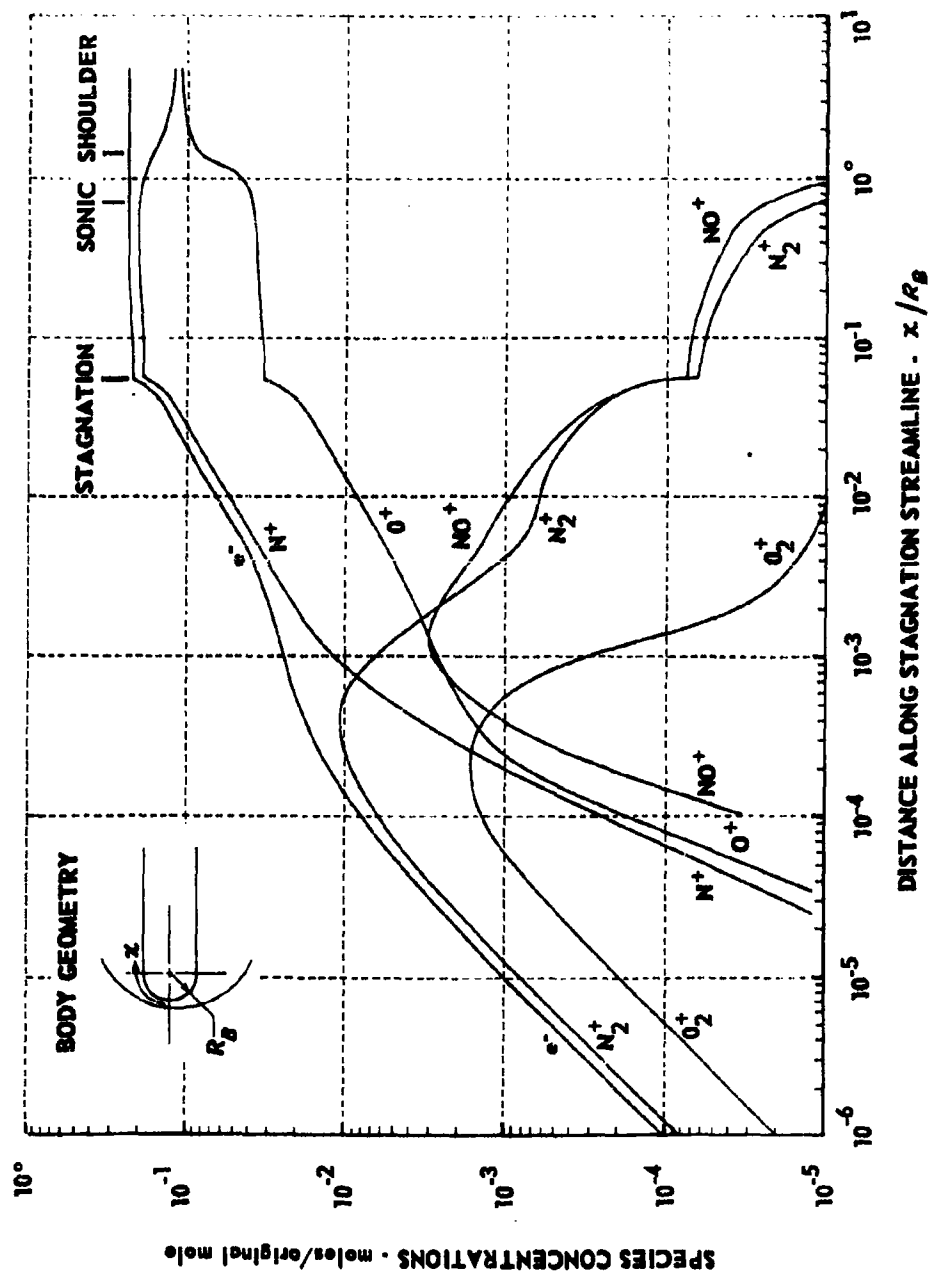
Figure 11 IONIZATION PROFILES ALONG STREAM SURFACE ABOUT A HEMISPHERE - CYLINDER

(VEL = 36 Kft/sec; ALT = 200 Kft; R_B = 1 foot)

AF-1500-A-1
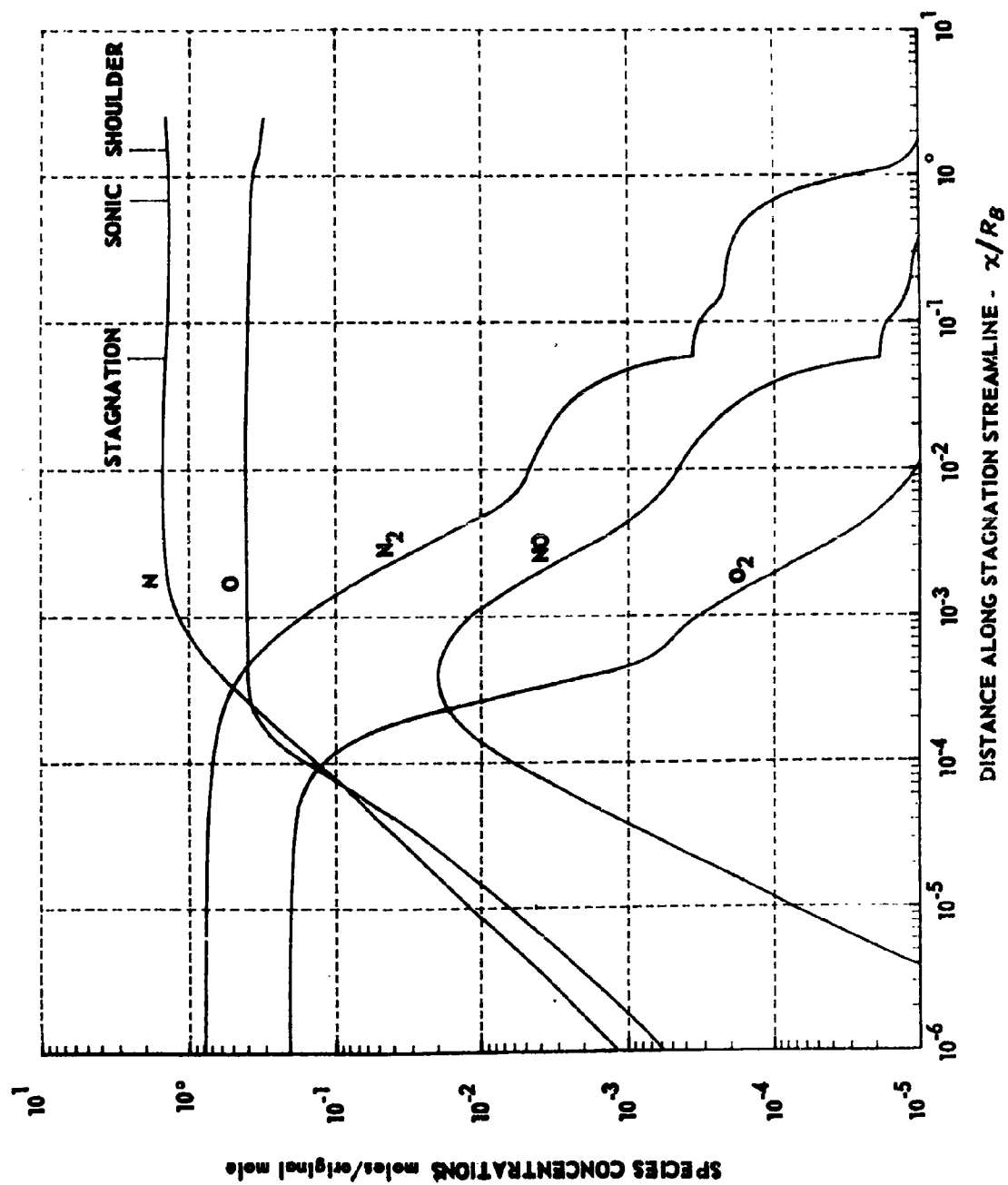
Figure 12   NEUTRAL PARTICLE DISTRIBUTIONS ALONG STAGNATION STREAMLINE FOR A HEMISPHERE
CYLINDER BODY (VEL = 36 Kft/sec; ALT = 200 Kft; R_B = 1 foot)
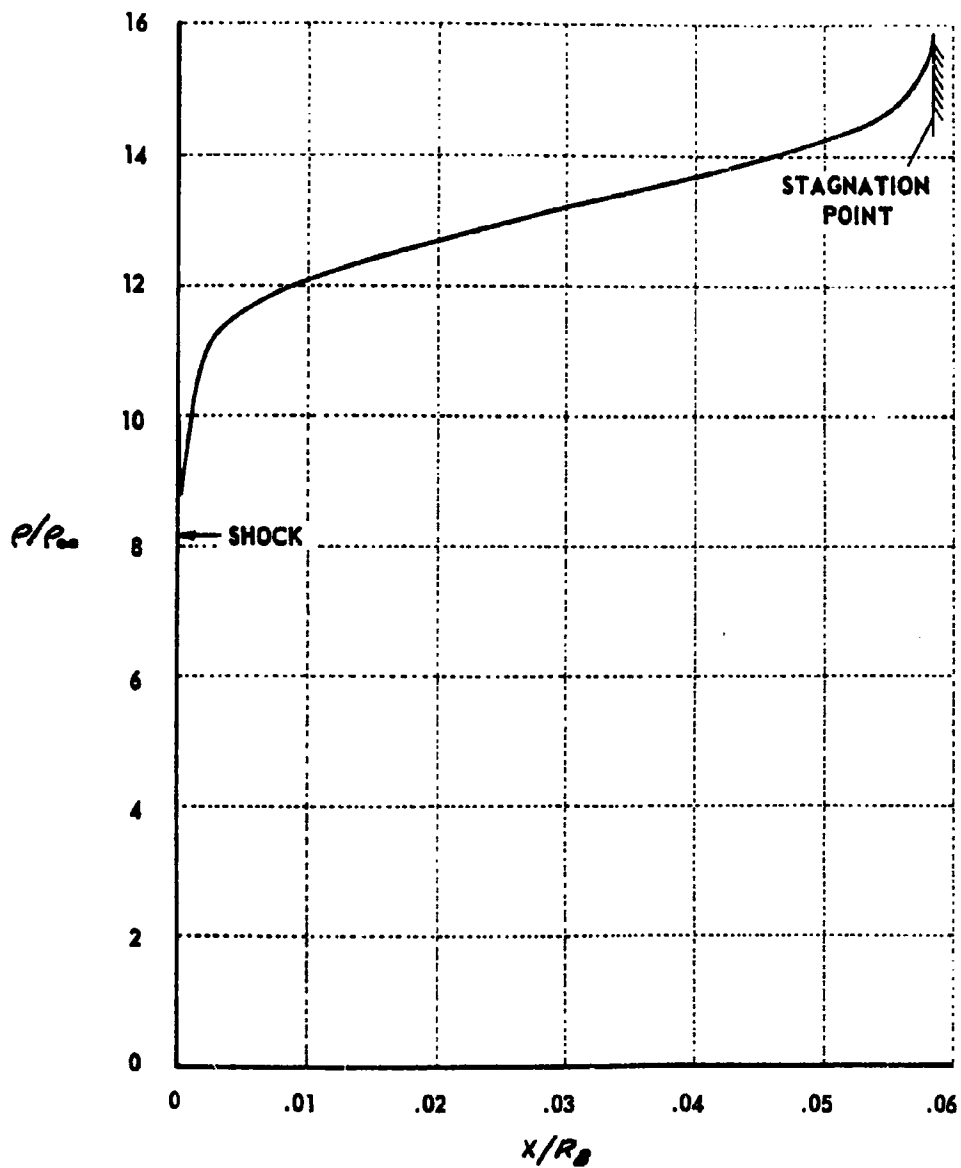
63   AF-1500-A-1
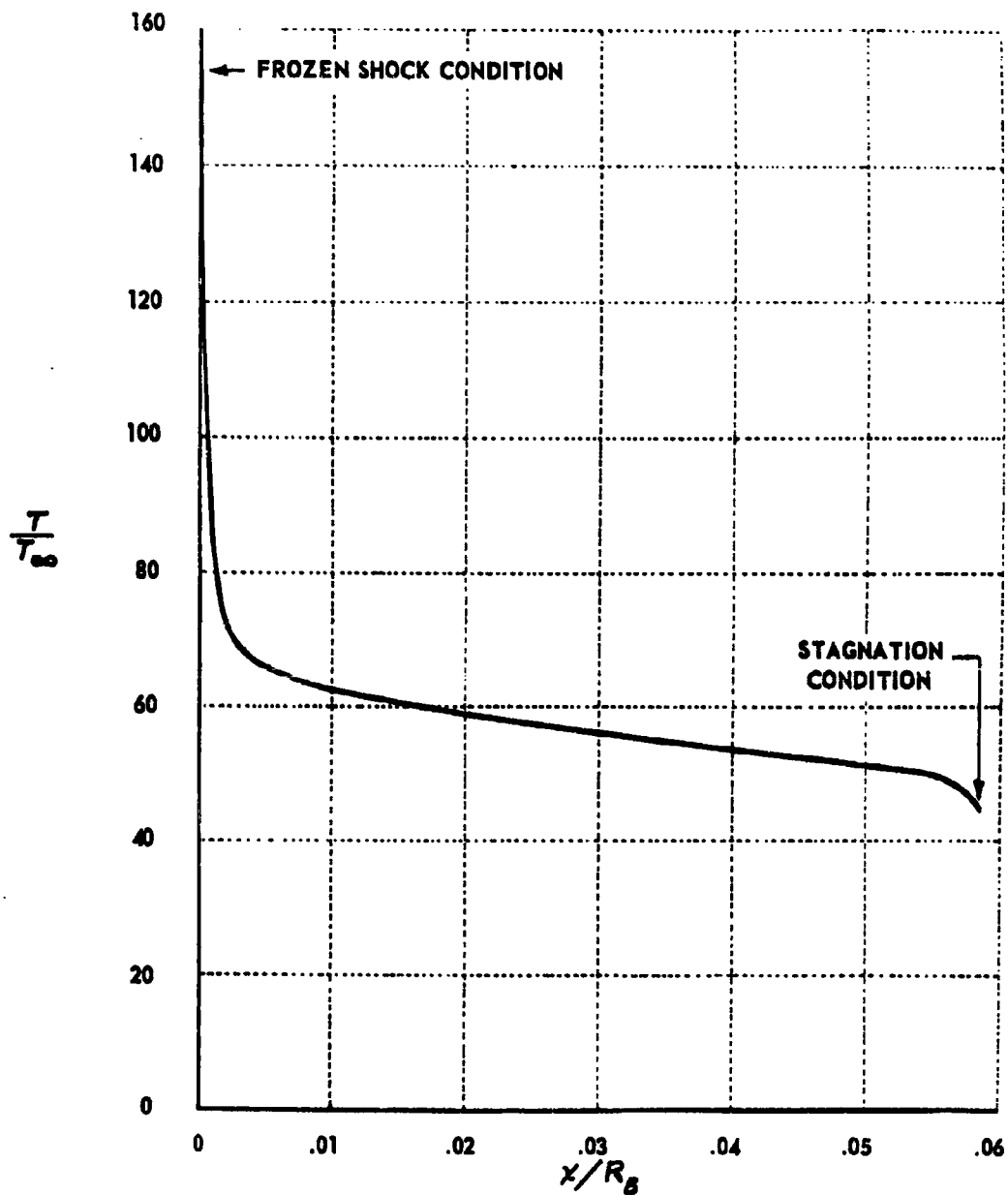
Figure 13a TEMPERATURE DISTRIBUTION ALONG STAGNATION
STREAMLINE IN THE SHOCK WAVE DETACHMENT
ZONE OF A HEMISPHERE-CYLINDER BODY (VEL = 36
Kft/sec; ALT = 200 Kft; R_B = 1 foot, T_∞ = 249°K)

64   AF-1500-A-1
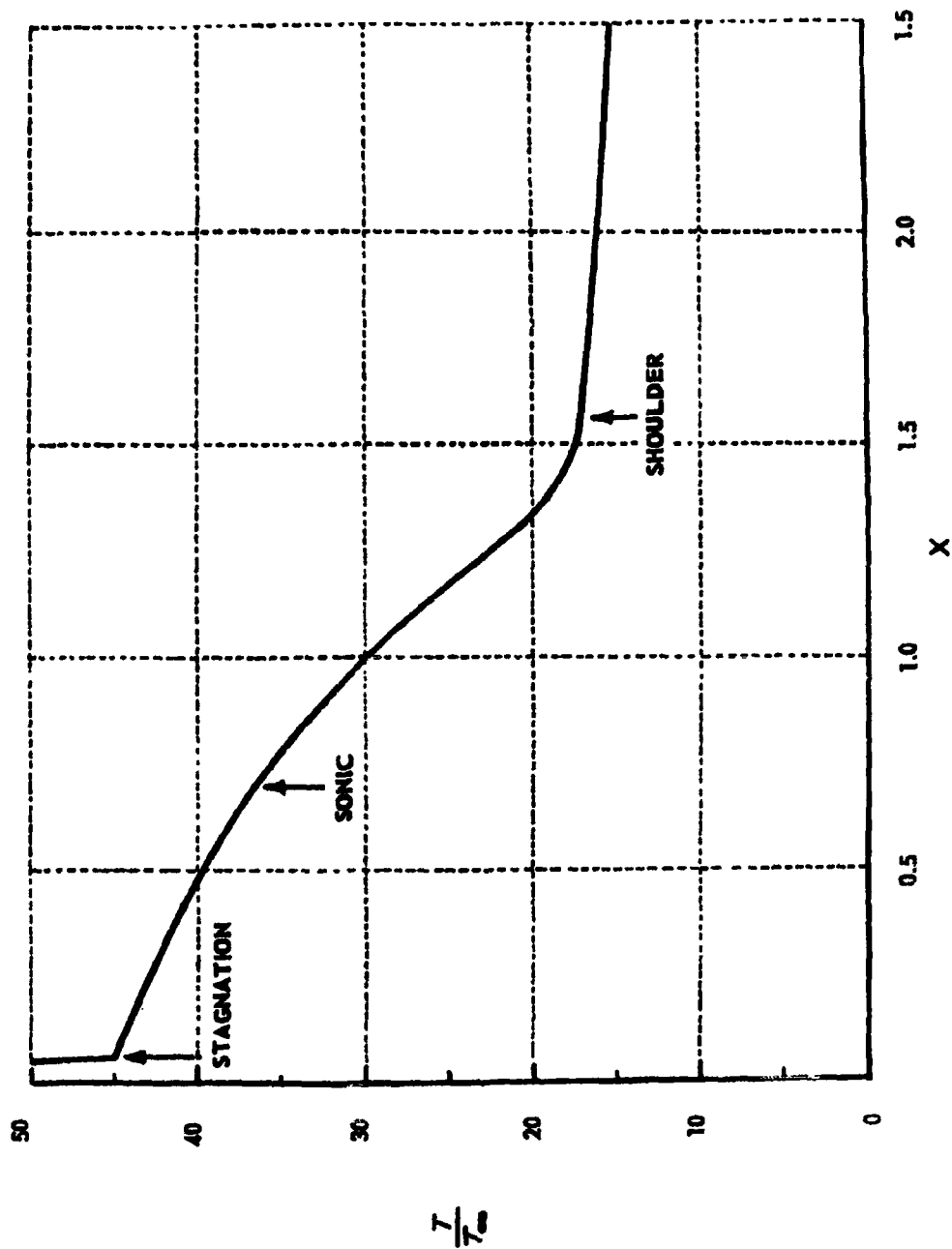
Figure 13b TEMPERATURE DISTRIBUTION ABOUT NOSE AND AFTERBODY OF A HEMISPHERE-CYLINDER (VEL = 36 Kft-sec; ALT = 200 Kft; R_B = 1 foot, T_∞ = 249°K)

65

Figure 14a DENSITY DISTRIBUTION ALONG STAGNATION STREAMLINE IN
THE SHOCK WAVE DETACHMENT ZONE OF A HEMISPHERE
CYLINDER BODY (VEL = 36 Kft/sec; ALT = 200 Kft;
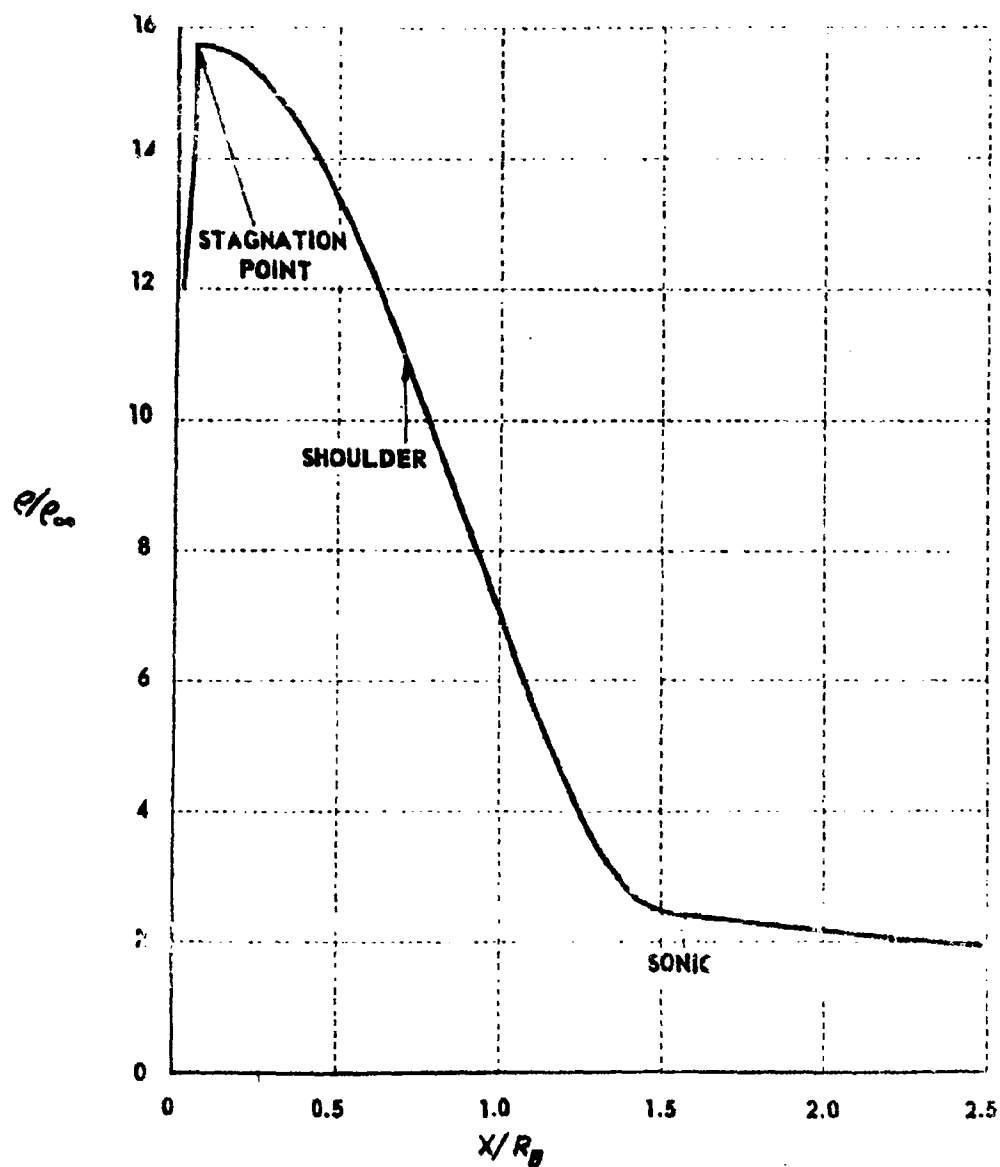R_B = 1 foot), ρ_∞ = 3.18 X 10^{-7} gm/cm^3)

66   AF-1500-A-1

Figure 14b   DENSITY DISTRIBUTION ABOUT NOSE AND AFTERBODY OF A
HEMISPHERE-CYLINDER (VEL = 36 Kft/sec; ALT = 200 Kft;
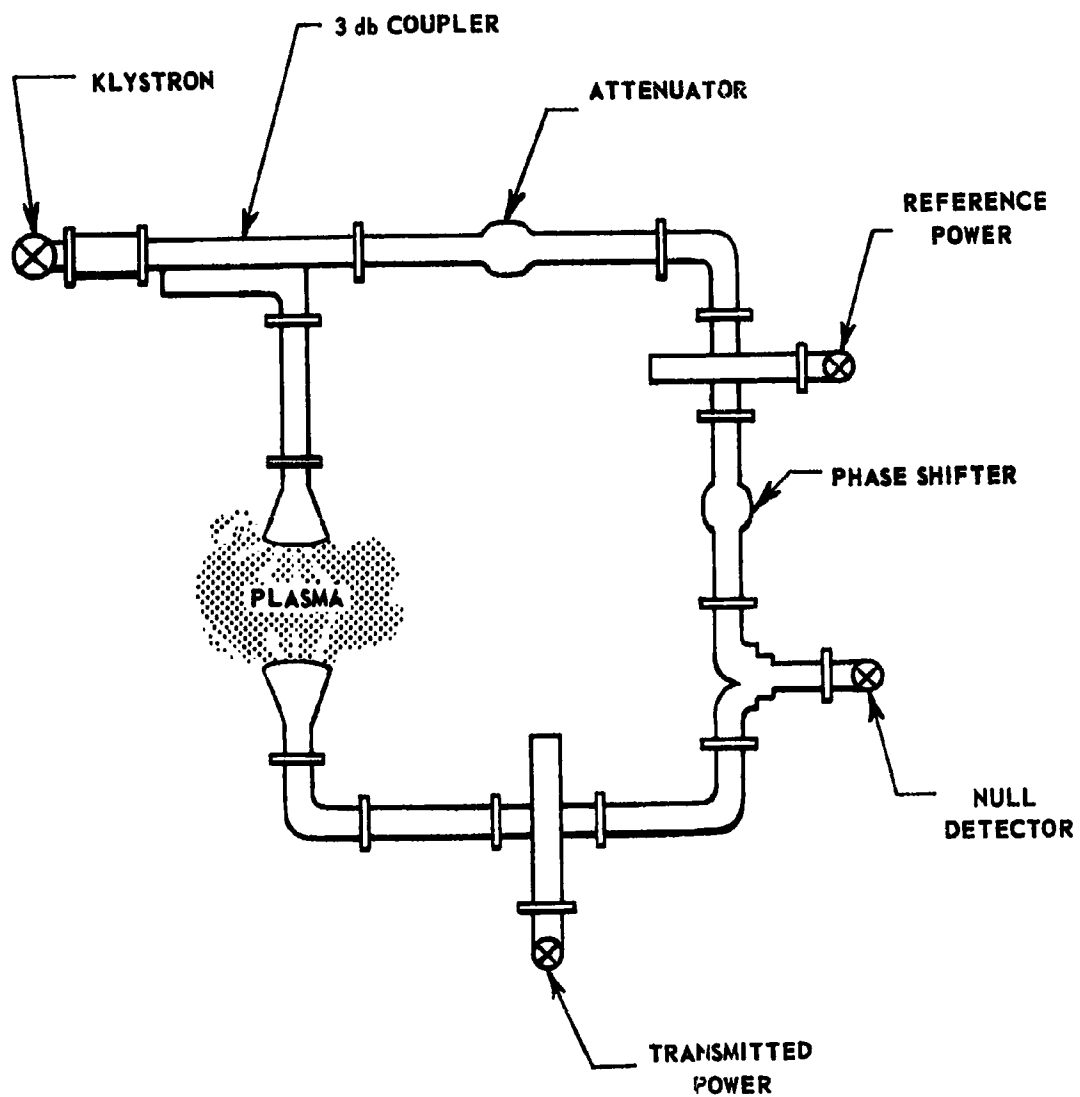R_B = 1 foot; ρ_∞ = 3.18 X 10^{-7} gm/cm^3)

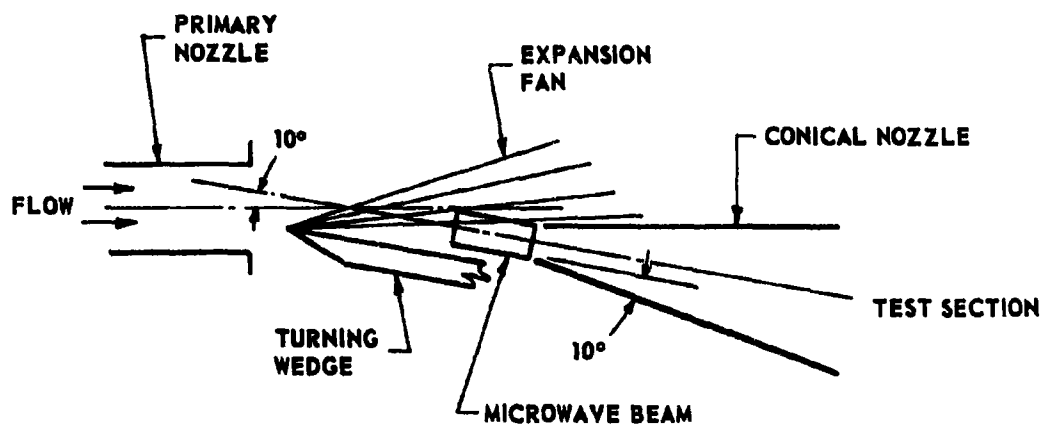Figure 15a MICROWAVE INTERFEROMETER SCHEMATIC

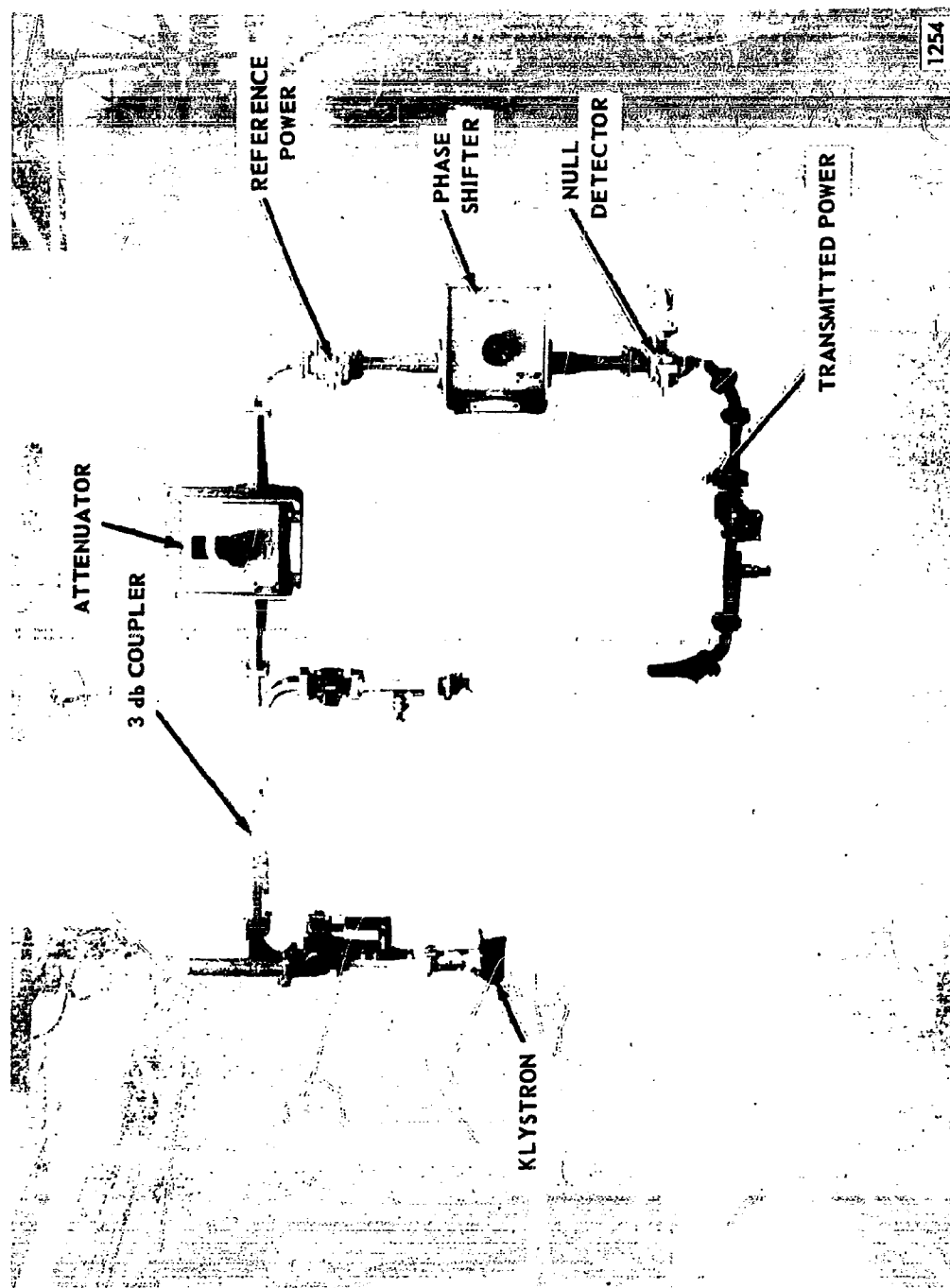AF-1500-A-1

Figure 15b   MICROWAVE INTERFEROMETER LOCATION

AF-1500-A-1

Figure 16 PHYSICAL ARRANGEMENT OF MICROWAVE INTERFEROMETER

AF-1500-A-1

RESERVOIR

SYMBOL	PRESSURE RANGE atm		
▽	20	to	30
○	75	to	100
◇	150	to	250
▲	350	to	450
□	640	to	720

PREDICTED ELECTRON DENSITIES
USING REACTION 10, FOR VARIOUS
RESERVOIR PRESSURES
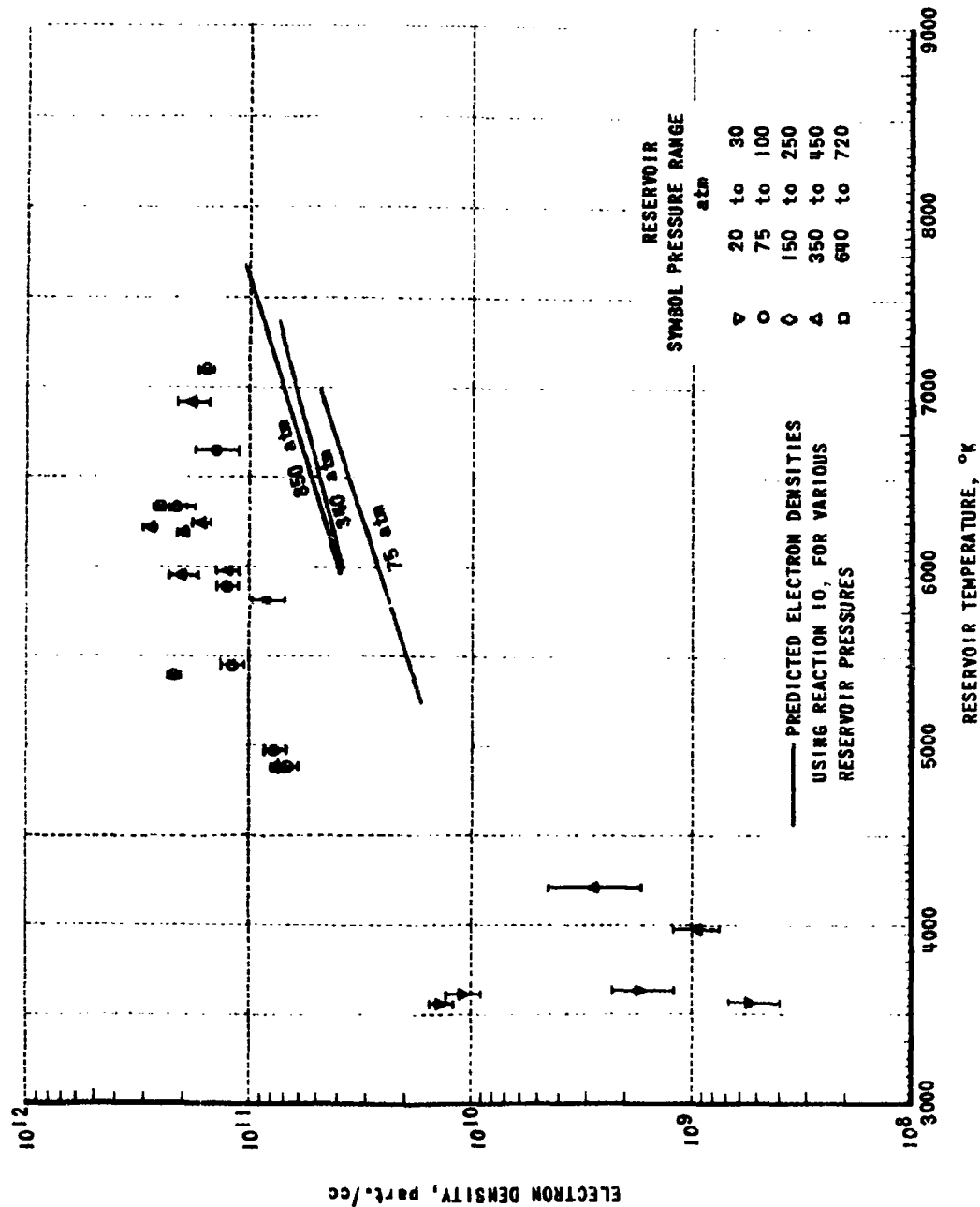
RESERVOIR TEMPERATURE, °K

Figure 17   ELECTRON DENSITY AT MICROWAVE STATION
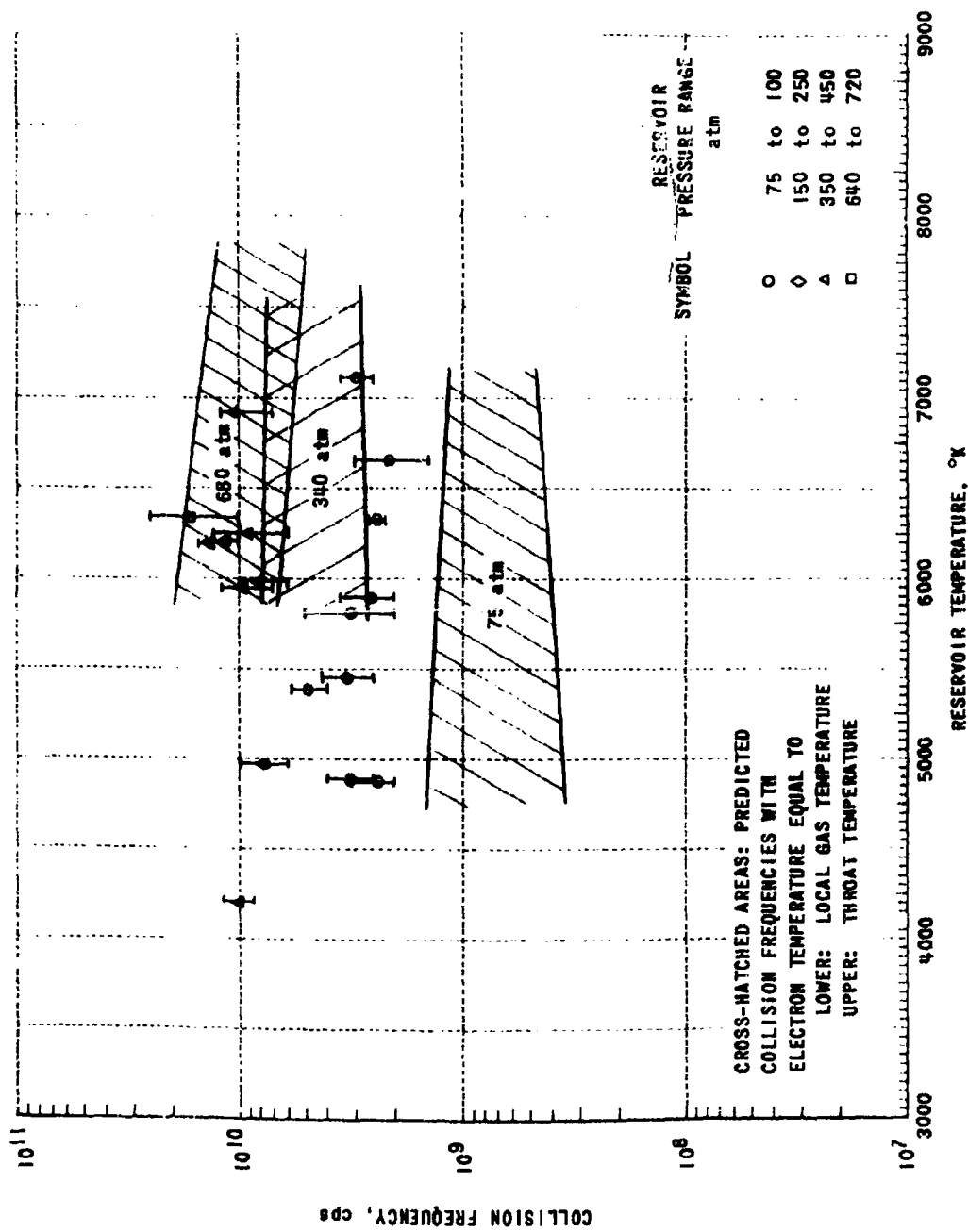IN SHOCK TUNNEL NOZZLE

71

Figure 18 ELECTRON COLLISION FREQUENCY AT MICROWAVE STATION
IN SHOCK TUNNEL NOZZLE

AF-1500-A-1